Research Article

Identification of new KCNT1-epilepsy drugs by *in silico,* cell, and *Drosophila* modeling

Michael G. Ricos PhD[1,†], Bethan A. Cole PhD [2,7,†], Rashid Hussain PhD[1,†], Grigori Y. Rychkov PhD[1,3,4], Zeeshan Shaukat PhD[1], Nadia Pilati PhD[5], Stephen P. Muench PhD[2,6], Katie J. Simmons PhD[2,6], Leanne M. Dibbens PhD[1], and Jonathan D. Lippiat PhD[2]

[1]Epilepsy Research Group, Clinical and Health Sciences, Australian Centre for Precision Health, University of South Australia, Adelaide, South Australia 5000, Australia. [2]School of Biomedical Sciences, Faculty of Biological Sciences, University of Leeds, Leeds LS2 9JT, UK. [3]School of Biomedicine, University of Adelaide, Adelaide, South Australia 5005, Australia. [4]South Australian Health and Medical Research Institute, Adelaide, South Australia 5005, Australia. [5]Autifony Srl, Istituto di Ricerca Pediatrica Citta' della Speranza, 35127 Padova, Italy. [6]Astbury Centre for Structural and Molecular Biology, University of Leeds, Leeds LS2 9JT UK. [7]Present address: Department of Biochemical and Cellular Pharmacology, Genentech, 103 DNA Way, South San Francisco, CA 94080, USA. [†]These authors contributed equally to this work.

Corresponding author: Dr Jonathan D. Lippiat

Corresponding author's address: School of Biomedical Sciences, Faculty of Biological Sciences, University of Leeds, Leeds LS2 9JT, UK

Corresponding author's phone and fax: +44 113 3434236, no fax

Corresponding author's e-mail address: J.D.Lippiat@leeds.ac.uk

Corresponding author: Prof. Leanne M. Dibbens

Corresponding author's address: Epilepsy Research Group, Clinical and Health Sciences, Australian Centre for Precision Health, University of South Australia, Adelaide, South Australia 5000, Australia,

Corresponding author's phone and fax: +61 8 830 21124

Corresponding author's e-mail address: Leanne.Dibbens@unisa.edu.au

Running head: KCNT1 channel inhibition by clinically-used drugs

Number of characters in title: 86

Number of characters in running head: 49

Number of words in abstract: 250

Number of words in Introduction: 427

Number of words in Discussion: 1194

Number of words in main text: 4739

Number of figures: 6 (5 color)

Number of tables: 1

Summary for Social Media If Published:

X handles: @drjonlippiat, @leanne_dibbens, @chmkjs, @beth_aimee_cole, @stemuench

Gain-of-function *KCNT1* variants cause severe childhood epilepsy that is presently not controlled by current medication. We used computational approaches to predict which drugs might reduce the activity of the potassium channel encoded by *KCNT1* and analyzed their effects in cellular and animal models. This study identified four drugs that inhibited KCNT1 channels, of which two reduced seizure-like behavior in *Drosophila* models and one emerged as the lead candidate drug, which may have beneficial effects in patients with *KCNT1*-associated epilepsy.

ABSTRACT

Objective: Hyperactive KCNT1 potassium channels, caused by gain-of-function mutations, are associated with a range of epilepsy disorders. Patients typically experience drug-resistant seizures and in cases with infantile onset, developmental regression can follow. KCNT1-related disorders include epilepsy of infancy with migrating focal seizures and sleep related hypermotor epilepsy. There are currently no effective treatments for KCNT1-epilepsies, but suppressing over-active channels poses a potential strategy.

Methods: Using the KCNT1 channel structure we *in silico* screened a library of known drugs for those predicted to block the channel pore to inhibit channel activity. Cellular KCNT1 channel inhibition was analyzed using electrophysiology and *Drosophila* bang-sensitive assays were used to analyze seizure suppression. Brain penetration of one drug was analyzed using liquid chromatography–mass spectrometry in mouse.

Results: Eight known drugs were investigated *in vitro* for their effects on patient-specific mutant KCNT1 channels, with four drugs showing significant reduction of K^+ current amplitudes. The action of the four drugs was then analyzed *in vivo* and two were found to reduce the seizure phenotype in humanized *Drosophila* KCNT1-epilepsy models. One drug, antrafenine, was shown to cross the blood-brain barrier in mice.

Interpretation: This study identified a known drug, antrafenine that reduces KCNT1 channel activity, reduces seizure activity in *Drosophila*, and crosses the blood-brain barrier in mouse, suggesting its potential applicability as a new treatment for KCNT1-epilepsy. The sequential *in silico*, *in vitro* and *in vivo* mechanism-based drug selection strategy used here may have broader application for other human disorders where a disease mechanism has been identified.

Key words: KCNT1; epilepsy; developmental and epileptic encephalopathy; sleep-related hypermotor epilepsy; epilepsy of infancy with migrating focal seizures; drug repurposing

INTRODUCTION

Mutations in *KCNT1* are associated with a range of drug-resistant epileptic and developmental neurological disorders. These include severe forms of epilepsy with onset in infancy, including epilepsy of infancy with migrating focal seizures (EIMFS) and later onset focal epilepsies, including sleep-related hypermotor epilepsy.[1-4] The KCNT1 potassium channel subunit is expressed widely in the central nervous system and is activated primarily by intracellular sodium and weakly by depolarisation.[5, 6] *KCNT1* mutations are heterozygous missense changes in the KCNT1 potassium channel subunit and increase channel activity. Accumulating evidence indicates that reduced excitability of inhibitory neurons associated with *KCNT1* mutations may be involved in hyperexcitability and seizures.[7-12]

Because *KCNT1*-associated disorders involve increased KCNT1 channel activity in the central nervous system, its suppression is the basis of proposed therapeutics. Until recently, the only pharmacological agents known to inhibit KCNT1 channels were the non-selective cation channel inhibitors quinidine, bepridil, and clofilium,[13, 14] each of which have potent effects on the cardiac action potential. Quinidine, a class 1a antiarrhythmic, has been assessed in *KCNT1*-associated disorders, but therapeutically-effective dosing is limited by its inhibition of cardiac ion channels and dangerous effects on the heartbeat.[15] Because of this, attempts have been made to identify novel KCNT1 inhibitors that are more potent and selective over other ion channels.[16-18] Although they are yet to reach clinical use, the efficacy of KCNT1 inhibitors in suppressing electrical activity in mouse models of epilepsy is particularly encouraging.[17-20] Clinically, there have been case reports of KCNT1 epilepsy patients whose seizures have been reduced with the antitussive drugs tipepidine and dextromethorphan,[21] the former of which has since been found to inhibit KCNT1 channels[20], and by fluoxetine, which in addition to several other ion channels has now been found to inhibit KCNT1[22, 23].

We hypothesized that existing drugs could be identified that have previously unknown KCNT1 channel inhibition as an off-target effect. We have previously utilized virtual high throughput screening to identify compounds predicted to occupy the pore in the structure of the chicken KCNT1 channel, generated using cryogenic electron microscopy (cryo-EM).[16, 24] Since this approach successfully identified novel inhibitors of the human KCNT1 channel,[16] we repeated this using a library of known drugs. Here, we describe *in vitro* KCNT1 inhibition as a novel property of four identified

drugs and demonstrate the efficacy of two in *in vitro* and *in vivo* model systems. In both cellular and *Drosophila* models, we have used several common mutations found in patients with *KCNT1* epilepsy, involving different functional domains of the channel. Thus, these drugs may potentially be effective for a range of patients with different clinical phenotypes.

METHODS

Virtual screening and drug selection

The intracellular pore region of the chicken KCNT1 channel cryo-EM structure (PDB:5U70)[24] assigned for docking studies was based upon the predicted binding of other inhibitors.[16] A 25 Å clip of the structure around these residues was used as the receptor for docking using Glide (Schrödinger, Release 2020-2).[25] The KCNT1 PDB file was prepared using the Protein Preparation Wizard in the Schrödinger Maestro Graphical User Interface (GUI). The academic version of the DrugBank library of known drug molecules (https://www.drugbank.com/academic_research) was downloaded and prepared using the OMEGA module[26] of OpenEye software (OMEGA version 2.5.1.4 OpenEye Scientific Software) to produce energy-minimized 3D structures before importing into Maestro GUI. Glide standard precision screening mode was used to predict the binding pose of each ligand. Drugs were ranked based on predicted binding affinity, likely membrane permeability, and commercial availability. To predict blood-brain-barrier permeability and CNS activity, the drug structures were created in Maestro, treated with LigPrep using OPLS forcefield, and molecular descriptors were calculated using QikProp (all Schrödinger, Release 2024-3).

Molecular biology

To replicate the heterozygous nature of *KCNT1*-associated disorder and obtain channels comprising wild-type (WT) and mutated subunits, a concatemeric approach was taken. To generate human KCNT1 concatemers, plasmids termed

donor and recipient were generated from the pcDNA6-KCNT1 construct used previously[16] and empty pcDNA6 V5/His6 vector (Invitrogen) using standard polymerase chain reaction (PCR) and cloning techniques. The insert of the donor construct comprised the KCNT1 coding sequence that lacked a start codon and preceded by bases encoding a GGGSGGGS linker. A second donor construct was generated by mutagenesis of this construct, replacing the linker sequence with "self-cleaving" T2A motif from the *Thosea asigna* virus (GSGEGRGSLLTCGDVEENPG),[27] which exhibits efficient cleavage in CHO cells.[28] The recipient construct was generated by deleting the stop codon and introducing a unique XhoI site. Sequences containing disease mutation Y796H were subcloned into these constructs from a plasmid used previously.[16] All sequences generated by PCR were confirmed by Sanger sequencing (Genewiz, Takeley, UK). Finally, the concatemeric construct was generated by subcloning the XhoI/AgeI fragment from the donor plasmid, containing the in-frame linker and complete subunit sequence into the same sites in the recipient plasmid. Recombination-deficient competent *E. coli* cells and 32ºC incubation temperature were used to reduce the frequency of deletions between identical sequences in the plasmid, which was confirmed by restriction analysis. For other experiments, constructs with WT, G288S, R398Q or R928C mutant forms of KCNT1 cDNA, tagged with YFP-6His in the pCMV-entry vectors, were described previously.[10]

Cell culture and transfection

Chinese hamster ovary (CHO) cells were cultured in Dulbecco's modified Eagle's Medium (ThermoFisher, UK) supplemented with 10% (v/v) fetal bovine serum, 50 U/ml penicillin and 0.05 mg/ml streptomycin, and incubated at 37°C in 5% CO_2 atmosphere. For whole cell recording of WT/Y796H KCNT1, CHO cells were transiently co-transfected with concatemeric WT/Y796H and EYFP as described previously.[29] For electrophysiological experiments, cells were plated onto borosilicate glass cover slips and used 2-4 days later. Human embryonic kidney 293T cells (HEK293T) were cultured in the same manner, but with medium supplemented with 2 mM L-glutamine, and 1% (v/v) non-essential amino acids. For excised inside-out recording of homomeric WT or mutant YFP-tagged KCNT1, HEK293T cells plated on glass cover slips were transfected using Attractene Transfection Reagent (Qiagen, Germany) according to the manufacturer's instructions and used 2-3 days later.

Electrophysiology

Whole cell recordings from transiently-transfected CHO cells were conducted at room temperature and analyzed as described previously.[29] The pipette (intracellular) solution contained, in mM, 100 K-Gluconate, 30 KCl, 10 Na-Gluconate, 29 Glucose, 5 EGTA and 10 HEPES, adjusted to pH 7.3 with KOH and the bath (extracellular) solution contained, in mM, 140 NaCl, 1 $CaCl_2$, 5 KCl, 29 Glucose, 10 HEPES and 1 $MgCl_2$, adjusted to pH 7.4 with NaOH. For current-voltage and conductance-voltage analysis of the concatemeric constructs, cells were held at -80 mV and 400 ms pulses were applied to voltages between -100 and 80 mV. Conductance values (G) with each voltage pulse (V) were obtained by dividing the peak steady-state current by the driving force (command voltage minus the measured reversal potential). Conductance-voltage data were fit by a Boltzmann function, $G = (G_{max} - G_{min})/(1+e^{(V-V_{½})/k)}) + G_{min}$, where G_{max} and G_{min} are the maximum and minimum conductance values, $V_{½}$ the half-maximal activation voltage, and slope k. The liquid junction potential was calculated and was used to correct voltage values after data collection. Inhibition by drugs, which were obtained from commercial sources, was determined from currents evoked by 500 ms voltage ramps from -100 to 0 mV at 0.2 Hz as described previously.[16] Initially drugs (10 mM in DMSO), were diluted to 10 μM in bath solution and applied via gravity perfusion for 2 min, followed by at least 2 min wash with drug-free solution prior to addition of the next drug. Drugs that exhibited inhibition at 10 μM were analyzed further by concentration-response: $G/G_C = (1 + ([B]/IC_{50})^H)^{-1} + c$, where G is the conductance measured as the slope of the current between -60 and 0 mV evoked by the voltage ramp in the presence of the inhibitor, G_C is the control conductance in the absence of inhibitor, $[B]$ is the concentration of the inhibitor, IC_{50} the concentration of inhibitor yielding 50% inhibition, H the slope, and c the residual conductance.

Inside-out patch clamp recordings were made at room temperature (23°C) from transiently-transfected HEK293T cells as described previously.[11] The pipette solution contained, in mM, 140 NaCl, 4 KCl, 2 $CaCl_2$, 2 $MgCl_2$ and 10 HEPES adjusted to pH 7.4 with NaOH. After achieving the inside-out configuration, the intracellular face of the membrane was constantly perfused with a solution containing, in mM, 35 NaCl, 110 KCl, 0.2 EGTA and 10 HEPES adjusted to pH 7.3 with KOH. Drug stock solutions of 5-20 mM in DMSO were first diluted in ethanol (1:10) and then in electrophysiological solution. KCNT1 currents were recorded using two voltage protocols, depending on the number of active channels in the patch before drug application. Macroscopic currents (number of active channels >15) were recorded in response to 100 ms voltage ramps between -120 and 120 mV applied every 2 s from a holding potential

of -78 mV. The average current amplitudes between 0 and 40 mV were used for the analyses and constructing the concentration-response curves. With a lower number of active channels in the patch (3 – 15), current traces were recorded in response to 15 s voltage steps to -20, 0 and 20 mV from a holding potential of -78 mV. Currents recorded at each voltage and each drug concentration were averaged over the duration of the trace and normalized to the average amplitudes of the corresponding current traces in drug-free solution. The normalized data for all three voltage steps were then averaged for each drug concentration and used to build the concentration-response curves (see Supplementary Fig. 3). To determine the $IC_{50,}$ data were fitted with Hill equation as described previously[11]. Single channel data were analyzed using Ana software developed by Dr Michael Pusch (Istituto di Biofisica, Genova, Italy) (http://users.ge.ibf.cnr.it/pusch/programs-mik.htm). In patch clamp data 'n' represents number of cells, and all experiments were repeated using cells from a minimum of two separate transfections.

Drosophila KCNT1-epilepsy models

The *Drosophila melanogaster* lines carrying the wild type human *KCNT1* transgene (NM_020822_3) or *KCNT1* mutant G288S, R398Q or R928C transgene placed downstream of the yeast UAS promoter, have been described previously.[11] Wild type or mutant human UAS-*KCNT1* flies were crossed to flies expressing the GAL4 transcriptional activator under the control of the *GAD1* promoter (GABAergic driver, Bloomington stock number 51630 P2) to drive expression of KCNT1 in GABAergic neurons, involved in neuronal inhibition.[11]

Bang-sensitive behavioral seizure assays in Drosophila

The bang-sensitive behavioral assay (also known as banging assay) was used to test for the presence of a seizure phenotype in *Drosophila*.[11, 30] Experiments were performed and scored as previously described[11] with a minimum of 50 *Drosophila* tested for each genotype and drug concentration.

Analysis of the effects of selected drugs on seizure activity in Drosophila

Four drugs were selected for *in vivo* analysis to determine their effects on the seizure phenotypes in transgenic *Drosophila* lines with human mutant KCNT1 channels. Bepridil, a non-selective KCNT1 inhibitor was included for comparison. *Drosophila* food with and without drugs was prepared as previously described.[11] All chemicals were obtained from Sigma-Aldrich (Gillingham, UK) apart from antrafenine hydrochloride (Toronto Research Chemicals, Canada) and regorafenib (USP, Germany).

Drosophila crosses were set up, and the resulting embryos were collected, as previously described (Hussain et al 2024). A range of concentrations of each drug dissolved in *Drosophila* food, between 0.001 µM and 1 µM, were used in the experiments. Multiple replicates were performed for each dosage of the drugs and controls. Controls were Vehicle Control (VC) which was the normal food with just the solvent ethanol present (1 µl/1 ml) in the *Drosophila* food, and Normal Food control (NF) where no drug or solvent (ethanol) was added in the *Drosophila* food.

Statistical analysis of Drosophila studies

In all experiments, experimenters were not blinded to variants or treatments, nor were samples randomly assigned to groups. Sample sizes were not calculated in advance and no data were excluded from the analysis. Data were analyzed using GraphPad Prism 9 software (San Diego, CA, USA). All values are reported as mean ± standard error (SEM). All data passed normality and lognormality Shapiro-Wilk tests, determined by GraphPad Prism 9. In the experiments analyzing the effects of drugs in *Drosophila*, statistical significance of differences between groups was determined using Brown-Forsythe and Welch's ANOVA tests (Supplementary Table 3), assuming non-equal SDs, followed by Dunnett's multiple comparisons tests (GraphPad Prism 9). The results of the Dunnett's multiple comparisons tests are shown in Supplementary Table 4, where '*N*' represents independent trials using independent fly crosses, with the total number of flies for each condition shown in brackets.

Pharmacokinetics and brain uptake of Antrafenine

Plasma pharmacokinetics and brain uptake of antrafenine was analyzed in male C57BL/6 mice. Antrafenine was administered intravenously at 1mg/kg and 3mg/kg into the tail vein and plasma was collected over a 24-hour sampling period (n=3 mice/time point). Following administration, brain was harvested at four times over 24 hours and snap frozen in dry ice and subsequently stored frozen (-80°C) until analysis. The concentration of antrafenine was determined using Liquid chromatography–mass spectrometry. The *in-vivo* study was conducted using established procedures in accordance with the Australian Code of Practice for the Care and Use of Animals for Scientific Purposes, and the study protocols were reviewed and approved by the Monash Institute of Pharmaceutical Sciences Animal Ethics Committee. See SI for detailed methods and results.

RESULTS

Identification and selection of drugs for functional evaluation

The predicted binding modes of the Drugbank compound library in the KCNT1 intracellular pore vestibule structure were computed and ranked by their docking score. These were further filtered by their clinical status as approved drugs, and manually selected based on their binding mode, commercial availability and computed hydrophobicity (clogP>3). Nine drugs were selected for functional assessment: indinavir, antrafenine, candesartan cilexetil, nelfinavir mesylate, regorafenib, dihydrotachysterol, atorvastatin, lifitegrast, and terconazole.

Generation of a cellular model of heterozygous assembly of wild-type and Y796H KCNT1 subunits

Several KCNT1 channel inhibitors differ in their potency between channels solely comprised of WT subunits or those with a disease-associated gain-of-function mutation.[16, 17, 31] Given the heterozygous dominant nature of *KCNT1*-disorders, we measured inhibition of channels containing both WT and mutant subunits. Initially, we generated concatemers by fusing two WT subunits with a flexible linker. In CHO cells, this yielded outwardly-rectifying currents that resembled WT KCNT1 (Fig. 1A), but with conductance-voltage relationships shifted to more negative potentials (Fig. 1C). In rodents, different *Kcnt1* mRNA transcripts are generated from alternative transcription initiation sites,

leading to variation in the amino terminus of the channel subunit and channels with altered activation kinetics.[32] We therefore reasoned that constraining the amino terminus of the second subunit in the concatemer may underlie this altered activity and the linker was replaced by a T2A "self-cleaving" motif. Expression of this construct in CHO cells resulted in similar currents, but with activation kinetics more closely resembling WT channels (Fig. 1). The second subunit in this concatemer was then replaced with one harboring the epilepsy-causingY796H mutation. Channels produced from this construct had activation half-maximal voltages intermediate of homomeric WT and Y796H KCNT1 channels. A summary of the activation kinetics of the monomeric and concatemeric channel currents is provided in Supplementary Table 1.

Functional evaluation of drugs in inhibiting WT/Y796H KCNT1 channels

Using the WT/Y796H KCNT1 construct to model "heterozygous" *KCNT1* pathogenic variants, the selected drugs were evaluated in whole-cell patch clamp experiments. Four of the drugs, antrafenine, atorvastatin, nelfinavir mesylate and regorafenib inhibited WT/Y796H KCNT1 channels expressed in CHO cells when tested at 10 μM concentration. Concentration-inhibition analysis yielded mean ± SEM IC_{50} of 1.30 ± 0.2 μM (n=5) for antrafenine, 2.86 ± 0.30 μM (*n*=5) for nelfinavir mesylate, 7.54 ± 0.99 μM (n=6) for atorvastatin, and 10.30 ± 1.25 μM (*n*=6) for regorafenib (Fig. 2A, B). Candesartan cilexetil appeared much less potent (Fig. 2B), and together with indinavir, dihydrotachysterol, liftegrast, and terconazole, which did not exhibit inhibition at 10 μM concentration (Fig. 2C), they were not studied any further.

Similar to the inhibitors that we previously identified by virtual screening,[16] these drugs were predicted to bind to the intracellular vestibule of the KCNT1 channel pore below the selectivity filter (Fig. 3, Supplementary Fig. 1). Each are predicted to make hydrophobic and hydrogen bond interactions with pore-lining amino acids, here provided as the equivalent amino acid and number in the human KCNT1 homolog. Antrafenine and atorvastatin are both predicted to make a hydrogen bonding interaction with the side chain of T314, which forms the intracellular-facing part of the selectivity filter, with atorvastatin making two additional hydrogen bonding interactions with the E347 side chain in the S6 segment. Nelfinavir and regorafenib are both predicted to hydrogen bond with the backbone carbonyl of F312, with nelfinavir also interacting with the side chain of T314. Antrafenine contains two and regorafenib contains one

terminal trifluoromethyl group. Similar to the predicted binding modes of BC12 and BC14,[16] we found that these terminal groups occupy a cavity formed between adjacent S6 segments and the pore helix. Antrafenine spans the pore, with the two trifluoromethyl groups at the opposite ends of the molecule occupying the equivalent cavities formed by opposite subunits in the KCNT1 tetramer. Since carrying out this docking, structures of human KCNT1 in several states, including with an inhibitor bound were published.[33] With the exception of atorvastatin, there is good agreement in the docking scores of these drugs between the chicken and inhibitor-bound human KCNT1 structures (Supplementary Table 2), with close conservation of both sequence and structure in the pore domain (Supplementary Fig. 2).

Inhibition of single human KCNT1 channels by the four prioritized drugs

Antrafenine, nelfinavir mesylate, atorvastatin and regorafenib were further analyzed by investigating their effects on unitary WT and R928C, G288S and R398Q mutant KCNT1 channels expressed in HEK293T cells in inside-out patches. The tight seal between the patch pipette and the cell was achieved in the control bath solution, after which the inside-out patch was excised and moved under the outlet of the gravity-fed perfusion system used to apply drugs to the intracellular face. Antrafenine and nelfinavir inhibited over 60% WT human KCNT1 channel activity at concentrations of 50 nM (Fig. 4A, B). The effects of atorvastatin and regorafenib on KCNT1 channels were less potent, with the drugs not fully inhibiting KCNT1 activity at concentrations of 10 μM (Fig. 4C, D). Each drug reduced the open probability of KCNT1 without affecting the single channel conductance (Fig. 4, insets). Antrafenine, nelfinavir mesylate and atorvastatin had similar inhibitory effects on WT and each of the R928C, G288S and R398Q mutant KCNT1 channels at the same concentrations (Fig. 5, Table 1, Supplementary Fig. 3).

In vivo analysis of the four prioritized drugs fed to Drosophila models of KCNT1-epilepsy

To analyze the effects of the four prioritized drugs on *KCNT1*-related seizures *in vivo*, we used our humanized *Drosophila* models of *KCNT1* epilepsy. The models contain human *KCNT1* with patient-specific mutations G288S, R398Q or R928C. *KCNT1* expression was under the control of the yeast UAS promoter and crossing to a line with the

GAL4 transcription factor under the control of a chosen promoter, enables tissue-specific expression of the transgene.[34] We have shown previously that expression of mutant KCNT1 channels in GABAergic inhibitory neurons gives a seizure phenotype in bang-sensitive assays and that these models can be used to analyze the effects of KCNT1-inhibiting drugs.[11]

Juvenile *Drosophila* (larvae) from the lines expressing G288S, R398Q, or R928C human KCNT1 channels, were fed each of the drugs and adult *Drosophila* were analyzed for seizure activity using bang-sensitive assays. Each mutant line was also raised on normal *Drosophila* food (NF) or normal *Drosophila* food containing the vehicle ethanol (VC) which was used to introduce each of the drugs to the *Drosophila* food. These two controls showed the baseline seizure activity of each of the mutant KCNT1 *Drosophila* lines (Fig. 6). As shown in Fig. 6, two of the drugs, antrafenine and nelfinavir mesylate, were seen to significantly reduce the seizure activity at concentrations 1 nM – 1 μM (inclusive) in each of the three *Drosophila* mutant *KCNT1* lines in a dose dependent manner (see Supplementary Tables 3 and 4 for statistics). The other two drugs, atorvastatin and regorafenib, did not show a significant effect on seizure activity in the G288S, R398Q or R928C mutant lines. Analysis of 1 μM atorvastatin was excluded due to reduced viability of adult flies at this concentration. The non-specific inhibitor bepridil was included for comparison and seen to exacerbate the seizure phenotype in each of the three *KCNT1* mutant lines (Fig. 6) as was observed with quinidine.[11] Nelfinavir mesylate showed the greatest reduction in seizure activity, followed by antrafenine. Previous publications on variable pharmacokinetics (Bergshoeff et al 2003) drug-drug interactions (ref) and limited brain uptake (ref),[35-37] raised concerns of the suitability of nelfinavir as a potential anti-epilepsy drug and it not further investigated in this study.

Investigation of blood-brain barrier penetration of antrafenine in mouse.

To further investigate the potential suitability of antrafenine as a drug for epilepsy, its ability to cross the blood brain barrier was analyzd in mice. Plasma pharmacokinetics and commensurate brain uptake of antrafenine were determined by Liquid Chromatography-Mass Spectrometry after intravenous administration of 3mg/kg antrafenine in C57BL/6 mice. The half-life of antrafenine in plasma was found to be 7.4 hours (Supplementary Table 6). At 4 hours after administration, the concentration of antrafeneine in brain was approximately 30% of that present in plasma, with a

mean plasma concentration of 47.5 nM (+5.9 nM SD) and a mean brain concentration of 13.9 nM (+3 nM SD) (Supplementary Table 7).

DISCUSSION

We have successfully used *in silico* screening to identify four existing drugs that inhibit KCNT1 channels at low micromolar potency in whole-cell patch clamp recordings, and importantly more potently than the known KCNT1 inhibitor quinidine. The outcomes from this approach are similar to those we obtained previously with a library of commercially available small molecules.[16] Since the four drugs have already been considered for therapeutic use, pharmacological and clinical data are available to inform whether they can be trailed for treating *KCNT1*-associated disorders. Using inside-out patch clamp recordings, antrafenine and nelfinavir were seen to inhibit 80 - 90% of the activity of the wild type and mutant human KCNT1 channels at 250 nM. This enhanced sensitivity, compared to whole-cell patch clamp, supports the idea that the drugs block the channel at the intracellular pore vestibule of the channel, either via the cytoplasm or directly from the lipid bilayer.

Based on the *in vitro* analysis and their inhibition of KCNT1 channels, the four drugs antrafenine, atorvastatin, nelfinavir mesylate, and regorafenib, were selected to be analyzed *in vivo* for their effects on the seizure phenotype in three humanized *Drosophila* models of *KCNT1*-epilepsy. *Drosophila* was chosen as an animal model as the key components in the regulation of neuronal excitability in humans and *Drosophila* are highly conserved.[38] Other *Drosophila* models of human genetic epilepsies include those for sodium channel *SCN1A*-related epilepsy[39] and Pyridox(am)ine 5′-phosphate oxidase (*PNPO*)-related epilepsy.[40] The relative ease of genetic manipulation, fast generation times and the low cost of housing make *Drosophila* attractive for modelling human epilepsy and for relatively rapid drug analyses.

The normal role of the KCNT1 channel is to reduce neuronal excitability and so it appears paradoxical that mutations leading to overactivity of the channel could contribute to neuronal hyperexcitability in epilepsy. However, this may be explained by accumulating evidence that overactivity of mutant KCNT1 channels in inhibitory neurons contributes to pathogenicity in KCNT1-epilepsy.[7-12.] Our *Drosophila* models expressed mutant human KCNT1

channels in inhibitory GABAergic neurons, exhibited a seizure phenotype, and were used for screening drugs for the ability to suppress seizures. *KCNT1* is widely expressed in the human brain (The Human Brain Atlas). However, expression of mutant KCNT1 channels in all neurons is embryonic lethal in *Drosophila*[11], therefore it is unknown if widespread expression of mutant KCNT1 channels would influence the seizure phenotype. Feeding of antrafenine or nelfinavir mesylate were found to significantly reduce the seizure phenotype in each *Drosophila* mutant *KCNT1* line, while atorvastatin and regorafenib did not. Nelfinavir was seen to reduce the seizure phenotype by 50% in *Drosophila* with G288S and R398Q and R928C. Antrafenine reduced the phenotype by at least 50% in G288S and R398Q, with a 25% reduction in R928C. The reduction of the seizure phenotype was found to be dose-dependent for each of these drugs, showing suppression at 0.001 µM, with the greatest effects at 0.1 µM or 1 µM in food. Based on physiological effective concentrations, the recommendation for drug screening in *Drosophila* is at concentrations between 0.1 µM - 10 µM added to the feeding substrate.[41] Antrafenine and nelfinavir were found to suppress seizures in the KCNT1 mutant *Drosophila* lines at concentrations between 0.001 µM -1.0 µM µM.[42] This suggests that the KCNT1 channel-blocking activities of antrafenine and nelfinavir are within an appropriate potential therapeutic range. Phenytoin, lamotrigine and valproate were seen to reduce seizures by approximately 30% in the Drosophila epilepsy model.[42] The reduction of seizures by approximately 25%-75% by antrafenine and nelfinavir in this study support their consideration as new drugs for epilepsy.

The two potential new drugs for treating people with *KCNT1*-epilepsy, antrafenine and nelfinavir mesylate, are yet to be trialed in patients for this indication. Non-selective cation channel blocking drugs, such as quinidine and bepridil have been shown to inhibit KCNT1 channels in *in vitro* experiments,[31, 43] with quinidine being trialed as a stratified treatment for *KCNT1* epilepsy.[44-47] However, quinidine has had mixed results in treating patients with worsening of seizures in some patients.[1, 48] The use of bepridil would be limited in clinical settings over safety concerns and was withdrawn for this reason.[49] We have shown that both bepridil (this study) and quinidine[11] exacerbate the seizure phenotype in our *Drosophila* models of *KCNT1*-epilepsy, most likely by inhibiting other cation channels that control neuronal excitability, highlighting the value of *in vivo* pre-clinical analysis for drug re-purposing. Interestingly, seizures were most exacerbated by bepridil in the R928C mutant line, suggesting mutation-specific differences in response to drugs and indicating a role for mutation-specific pharmacogenomics.

Nelfinavir mesylate and antrafenine showed significant reduction in seizure activity associated with all three *KCNT1* patient mutations R928C, R398Q and G288S when tested in our animal models. They also showed significant reduction of K^+ currents in HEK cells expressing the same three mutant channels, as well as channels comprised of WT and Y796H mutant KCNT1 subunits in CHO cells. These data suggests that these two drugs have the potential to inhibit a spectrum of mutant *KCNT1* channels found in patients and, if found to be clinically effective, could be new treatments for patients with a range of different *KCNT1* mutations. Apart from antrafenine, each of the KCNT1-inhibiting drugs described here are presently in clinical use. Atorvastatin (brand name Lipitor) is a competitive inhibitor of 3-hydroxy-3-methyl-glutaryl-coenzyme A (HMG-CoA) reductase, an enzyme involved in cholesterol synthesis, and is a statin used in the treatment of hyperlipidemia and hypercholesterolemia. Partial inhibition of hERG currents by atorvastatin at low micromolar concentrations have been reported and appear to affect hERG channel inactivation kinetics.[50] Regorafenib (brand name Stivarga) is an anticancer drug that targets receptor tyrosine kinases and is presently under clinical evaluation for treating brain tumors.[51] Of the drugs with efficacy in *Drosophila*, nelfinavir mesylate (brand name Viracept) is an HIV-1 protease inhibitor. It has been reported that this drug inhibits hERG potassium channels with an IC_{50} of 11.5 μM,[52] which could place patients at risk of arrhythmia. Its CNS penetrance is believed to be limited by its extrusion by P-glycoprotein in the blood-brain barrier, [53] which may prevent concentrations reaching levels required to inhibit KCNT1. Antrafenine (brand name Stakane) has analgesic and anti-inflammatory effects, but there is no record of its clinical availability or use since the mid-1980s. Pharmacokinetic studies of this drug are lacking, though a the QPlogBB score (Supplementary Table 2) is within range of drugs that cross the blood-brain barrier. In a clinical study with osteoarthritis patients, mean circulating plasma levels of 0.3 μM antrafenine were measured,[54] which is in the concentration range of KCNT1 channel inhibition reported here. We evaluated the pharmacokinetic properties of brain uptake of antrafenine in mouse and found significant penetration of antrafenine into the brain at concentrations close to 30% of those present in plasma. No toxic effects of antrafenine in mice were noted in this study, consistent with previous studies in mouse and rats,[55] and clinical studies have shown that the drug is well tolerated in humans at 900 mg/day.[54] Based on these findings, we consider antrafenine as the lead candidate new drug for KCNT1 epilepsy from this study. Seizure reduction efficacy in rodent models of *KCNT1* epilepsy will be required to justify its future clinical evaluation in patients with *KCNT1* epilepsy.

ACKNOWLEDGMENT

We thank Dr Emily Caseley (University of Leeds) for conducting molecular docking of drugs against the inhibitor-bound human KCNT1 structure. We thank the Monash University Centre for Drug Candidate Optimisation for conducting the antrafenine pharmacokinetic study in mice. We acknowledge support from a BBSRC-CASE PhD studentship (BB/M011151/1) in conjunction with Autifony Therapeutics Ltd (BAC), the Channel 7 Children's Research Foundation Grant 13435028 (LMD, GYR, ZS), and National and Health Medical Research Council of Australia (Senior Research Fellowship 1104718 and Project Grant 1125523 to LMD, and Ideas Grant 2028987 to LMD, GYR and RH).

AUTHOR CONTRIBUTIONS

LMD and JDL contributed to the conception and design of the study. MGR, BAC, RH, GYR, ZS, NP, SPM, KJS, LMD and JDL contributed the acquisition and analysis of data. All authors contributed to drafting the text or preparing the figures. MGR., BAC, and RH contributed equally to this work and should be considered as co-first authors.

CONFLICTS OF INTEREST

The authors declare that they have no conflicts of interest.

DATA AVAILABILITY

The data that support the findings of this study are available from the corresponding authors, upon reasonable request.

REFERENCES

1. Bonardi CM, Heyne HO, Fiannacca M, et al. KCNT1-related epilepsies and epileptic encephalopathies: phenotypic and mutational spectrum. Brain. 2021.
2. Heron SE, Smith KR, Bahlo M, et al. Missense mutations in the sodium-gated potassium channel gene KCNT1 cause severe autosomal dominant nocturnal frontal lobe epilepsy. Nat Genet. 2012 Nov;44(11):1188-90.
3. Barcia G, Fleming MR, Deligniere A, et al. De novo gain-of-function KCNT1 channel mutations cause malignant migrating partial seizures of infancy. Nat Genet. 2012 Nov;44(11):1255-9.
4. Lim CX, Ricos MG, Dibbens LM, Heron SE. KCNT1 mutations in seizure disorders: the phenotypic spectrum and functional effects. J Med Genet. 2016 Apr;53(4):217-25.
5. Yuan A, Santi CM, Wei A, et al. The sodium-activated potassium channel is encoded by a member of the Slo gene family. Neuron. 2003 Mar 6;37(5):765-73.
6. Bhattacharjee A, Gan L, Kaczmarek LK. Localization of the Slack potassium channel in the rat central nervous system. J Comp Neurol. 2002 Dec;454(3):241-54.
7. Shore AN, Colombo S, Tobin WF, et al. Reduced GABAergic Neuron Excitability, Altered Synaptic Connectivity, and Seizures in a KCNT1 Gain-of-Function Mouse Model of Childhood Epilepsy. Cell Rep. 2020 Oct 27;33(4):108303.
8. Gertler TS, Cherian S, DeKeyser JM, Kearney JA, George AL, Jr. K(Na)1.1 gain-of-function preferentially dampens excitability of murine parvalbumin-positive interneurons. Neurobiol Dis. 2022 Jun 15;168:105713.
9. Kuchenbuch M, Nabbout R, Yochum M, et al. In silico model reveals the key role of GABA in KCNT1-epilepsy in infancy with migrating focal seizures. Epilepsia. 2021 Mar;62(3):683-97.
10. Rychkov GY, Shaukat Z, Lim CX, et al. Functional Effects of Epilepsy Associated KCNT1 Mutations Suggest Pathogenesis via Aberrant Inhibitory Neuronal Activity. International journal of molecular sciences. 2022 Dec 1;23(23).
11. Hussain R, Lim CX, Shaukat Z, et al. Drosophila expressing mutant human KCNT1 transgenes make an effective tool for targeted drug screening in a whole animal model of KCNT1-epilepsy. Sci Rep. 2024 Feb 9;14(1):3357.
12. Wu J, Quraishi IH, Zhang Y, Bromwich M, Kaczmarek LK. Disease-causing Slack potassium channel mutations produce opposite effects on excitability of excitatory and inhibitory neurons. Cell reports. 2024 Mar 26;43(3):113904.

13. Yang B, Gribkoff VK, Pan J, et al. Pharmacological activation and inhibition of Slack (Slo2.2) channels. Neuropharmacology. 2006 Sep;51(4):896-906.

14. de Los Angeles Tejada M, Stolpe K, Meinild AK, Klaerke DA. Clofilium inhibits Slick and Slack potassium channels. Biologics. 2012;6:465-70.

15. Mullen SA, Carney PW, Roten A, et al. Precision therapy for epilepsy due to KCNT1 mutations: A randomized trial of oral quinidine. Neurology. 2018 Jan 2;90(1):e67-e72.

16. Cole BA, Johnson RM, Dejakaisaya H, et al. Structure-Based Identification and Characterization of Inhibitors of the Epilepsy-Associated K. iScience. 2020 May;23(5):101100.

17. Griffin AM, Kahlig KM, Hatch RJ, et al. Discovery of the First Orally Available, Selective K(Na)1.1 Inhibitor: In Vitro and In Vivo Activity of an Oxadiazole Series. ACS Med Chem Lett. 2021 Apr 8;12(4):593-602.

18. Spitznagel BD, Mishra NM, Qunies AM, et al. VU0606170, a Selective Slack Channels Inhibitor, Decreases Calcium Oscillations in Cultured Cortical Neurons. ACS Chem Neurosci. 2020 Nov 4;11(21):3658-71.

19. Di C, Wu T, Gao K, et al. Carvedilol inhibits neuronal hyperexcitability caused by epilepsy-associated KCNT1 mutations. Br J Pharmacol. 2025 Jan;182(1):162-80.

20. Guo Q, Gan J, Wang EZ, et al. Electrophysiological characterization of human KCNT1 channel modulators and the therapeutic potential of hydroquinine and tipepidine in KCNT1 mutation-associated epilepsy mouse model. Acta pharmacologica Sinica. 2025 Jan 27.

21. Takase C, Shirai K, Matsumura Y, et al. KCNT1-positive epilepsy of infancy with migrating focal seizures successfully treated with nonnarcotic antitussive drugs after treatment failure with quinidine: A case report. Brain & development. 2020 Sep;42(8):607-11.

22. Mosca I, Freri E, Ambrosino P, et al. Case report: Marked electroclinical improvement by fluoxetine treatment in a patient with KCNT1-related drug-resistant focal epilepsy. Front Cell Neurosci. 2024;18:1367838.

23. Trivisano M, Mosca I, Salimbene L, et al. Fluoxetine Treatment in Epilepsy of Infancy with Migrating Focal Seizures Due to KCNT1 Variants: An Open Label Study. Ann Neurol. 2025 Feb 21.

24. Hite RK, MacKinnon R. Structural Titration of Slo2.2, a Na+-Dependent K+ Channel. Cell. 2017 Jan;168(3):390-9.e11.

25. Friesner RA, Banks JL, Murphy RB, et al. Glide: a new approach for rapid, accurate docking and scoring. 1. Method and assessment of docking accuracy. Journal of medicinal chemistry. 2004 Mar 25;47(7):1739-49.

26. Hawkins PC, Skillman AG, Warren GL, Ellingson BA, Stahl MT. Conformer generation with OMEGA: algorithm and validation using high quality structures from the Protein Databank and Cambridge Structural Database. Journal of chemical information and modeling. 2010 Apr 26;50(4):572-84.

27. Kim JH, Lee SR, Li LH, et al. High cleavage efficiency of a 2A peptide derived from porcine teschovirus-1 in human cell lines, zebrafish and mice. PLoS One. 2011;6(4):e18556.

28. Chng J, Wang T, Nian R, et al. Cleavage efficient 2A peptides for high level monoclonal antibody expression in CHO cells. MAbs. 2015;7(2):403-12.

29. Cole BA, Kalli AC, Pilati N, Muench SP, Lippiat JD. A molecular switch in RCK2 triggers sodium-dependent activation of K(Na)1.1 (KCNT1) potassium channels. Biophysical journal. 2024 Jul 16;123(14):2145-53.

30. Song J, Tanouye MA. From bench to drug: human seizure modeling using Drosophila. Progress in neurobiology. 2008 Feb;84(2):182-91.

31. Rizzo F, Ambrosino P, Guacci A, et al. Characterization of two de novoKCNT1 mutations in children with malignant migrating partial seizures in infancy. Mol Cell Neurosci. 2016 Apr;72:54-63.

32. Brown MR, Kronengold J, Gazula VR, et al. Amino-termini isoforms of the Slack K+ channel, regulated by alternative promoters, differentially modulate rhythmic firing and adaptation. J Physiol. 2008 Nov 1;586(21):5161-79.

33. Zhang J, Liu S, Fan J, et al. Structural basis of human Slo2.2 channel gating and modulation. Cell reports. 2023 Jul 25;42(8):112858.

34. Brand AH, Perrimon N. Targeted gene expression as a means of altering cell fates and generating dominant phenotypes. Development. 1993 Jun;118(2):401-15.

35. Bergshoeff AS, Fraaij PL, van Rossum AM, et al. Pharmacokinetics of nelfinavir in children: influencing factors and dose implications. Antiviral therapy. 2003 Jun;8(3):215-22.

36. Capparelli EV, Sullivan JL, Mofenson L, et al. Pharmacokinetics of nelfinavir in human immunodeficiency virus-infected infants. The Pediatric infectious disease journal. 2001 Aug;20(8):746-51.

37. Mirochnick M, Stek A, Acevedo M, et al. Safety and pharmacokinetics of nelfinavir coadministered with zidovudine and lamivudine in infants during the first 6 weeks of life. Journal of acquired immune deficiency syndromes (1999). 2005 Jun 1;39(2):189-94.

38. Takai A, Yamaguchi M, Yoshida H, Chiyonobu T. Investigating Developmental and Epileptic Encephalopathy Using Drosophila melanogaster. Int J Mol Sci. 2020 Sep 3;21(17).

39. Dare SS, Merlo E, Rodriguez Curt J, Ekanem PE, Hu N, Berni J. Drosophila para (bss) Flies as a Screening Model for Traditional Medicine: Anticonvulsant Effects of Annona senegalensis. Front Neurol. 2020;11:606919.

40. Chi W, Iyengar ASR, Fu W, et al. Drosophila carrying epilepsy-associated variants in the vitamin B6 metabolism gene PNPO display allele- and diet-dependent phenotypes. Proc Natl Acad Sci U S A. 2022 Mar 1;119(9).

41. Pandey UB, Nichols CD. Human disease models in Drosophila melanogaster and the role of the fly in therapeutic drug discovery. Pharmacological reviews. 2011 Jun;63(2):411-36.

42. Fischer FP, Karge RA, Koch H, Voigt A, Weber YG, Wolking S. The fruit fly Drosophila melanogaster as a screening model for antiseizure medications. Frontiers in pharmacology. 2024;15:1489888.

43. Milligan CJ, Li M, Gazina EV, et al. KCNT1 gain of function in 2 epilepsy phenotypes is reversed by quinidine. Ann Neurol. 2014 Apr;75(4):581-90.

44. Bearden D, Strong A, Ehnot J, DiGiovine M, Dlugos D, Goldberg EM. Targeted treatment of migrating partial seizures of infancy with quinidine. Ann Neurol. 2014 Sep;76(3):457-61.

45. Chong PF, Nakamura R, Saitsu H, Matsumoto N, Kira R. Ineffective quinidine therapy in early onset epileptic encephalopathy with KCNT1 mutation. Ann Neurol. 2016 Mar;79(3):502-3.

46. Madaan P, Jauhari P, Gupta A, Chakrabarty B, Gulati S. A quinidine non responsive novel KCNT1 mutation in an Indian infant with epilepsy of infancy with migrating focal seizures. Brain Dev. 2018 Mar;40(3):229-32.

47. Dilena R, DiFrancesco JC, Soldovieri MV, et al. Early Treatment with Quinidine in 2 Patients with Epilepsy of Infancy with Migrating Focal Seizures (EIMFS) Due to Gain-of-Function KCNT1 Mutations: Functional Studies, Clinical Responses, and Critical Issues for Personalized Therapy. Neurotherapeutics. 2018 Oct;15(4):1112-26.

48. Xu D, Chen S, Yang J, Wang X, Fang Z, Li M. Precision therapy with quinidine of KCNT1-related epileptic disorders: a systematic review. Br J Clin Pharmacol. 2022 Aug 8.

49. Sasaoka S, Matsui T, Hane Y, et al. Time-to-Onset Analysis of Drug-Induced Long QT Syndrome Based on a Spontaneous Reporting System for Adverse Drug Events. PLoS One. 2016;11(10):e0164309.

50. Feng P, Zhao L, Guo F, et al. The enhancement of cardiotoxicity that results from inhibiton of CYP 3A4 activity and hERG channel by berberine in combination with statins. Chemico-biological interactions. 2018 Sep 25;293:115-23.

51. Mongiardi MP, Pallini R, D'Alessandris QG, Levi A, Falchetti ML. Regorafenib and glioblastoma: a literature review of preclinical studies, molecular mechanisms and clinical effectiveness. Expert reviews in molecular medicine. 2024 Apr 2;26:e5.

52. Anson BD, Weaver JG, Ackerman MJ, et al. Blockade of HERG channels by HIV protease inhibitors. Lancet (London, England). 2005 Feb 19-25;365(9460):682-6.

53. Salama NN, Kelly EJ, Bui T, Ho RJ. The impact of pharmacologic and genetic knockout of P-glycoprotein on nelfinavir levels in the brain and other tissues in mice. Journal of pharmaceutical sciences. 2005 Jun;94(6):1216-25.

54. Berry H, Coquelin JP, Gordon A, Seymour D. Antrafenine, naproxen and placebo in osteoarthritis: a comparative study. Br J Rheumatol. 1983 May;22(2):89-94.

55. Manoury PM, Dumas AP, Najer H, Branceni D, Prouteau M, Lefevre-Borg FM. Synthesis and analgesic activities of some (4-substituted phenyl-1-piperazinyl)alkyl 2-aminobenzoates and 2-aminonicotinates. Journal of medicinal chemistry. 1979 May;22(5):554-9.

FIGURE LEGENDS

Figure 1. Generation of an expression construct for heteromeric expression of WT and Y796H KCNT1 subunits. The concatemeric constructs encode two KCNT1 subunits, separated by either a tethered EGGGSGGGS motif or a T2A self-cleaving peptide between the first and second subunit. **A** Representative current traces recorded from non-transfected CHO cells using whole-cell patch clamp or with CHO cells transfected with constructs containing WT KCNT1 subunits in both the first and second position (WT-WT with a hyphen indicates the tethered concatemer; WT/WT with a slash indicates the cleavable T2A construct), Y796H KCNT1 in both the first and second positions (Y796H/Y796H), or WT in the first and Y796H KCNT1 in the second positions (WT/Y796H), as indicated. The dashed line indicates the zero-current levels. **B** Current-voltage and **C** Conductance-voltage relationships from the recorded currents. Mean data for monomeric WT KCNT1 (black) and Y796H (red) are indicated as dashed lines for comparison. Data are mean ± SEM (n= 6 cells for WT-WT and WT/Y796H; n=5 cells for WT/WT and Y796H/Y796H).

Figure 2. Functional evaluation of drugs with WT/Y796H KCNT1 channels expressed in CHO cells. A Representative traces and **B** mean ± SEM. concentration-dependent inhibition by active inhibitors. Antraf, antrafenine (*n*=5 cells); Regor, regorafenib (*n*=6 cells); Ator, atorvastatin (*n*=6 cells); Cand, candesartan (*n*=5 cells); Nelf, nelfinavir (*n*=5 cells). **C** Drugs inactive at 10 μM. Data are mean ± SEM WT/Y796H KCNT1 conductance measured as the slope of the current evoked by a voltage ramp to from -100 to 0 mV in the presence of 10 μM inhibitor, relative to control conductance prior to drug application. Dihydro, dihydrotachysterol (*n*=3 cells); Lift, liftegrast (*n*=3 cells); Indin, indinavir (*n*=3 cells); Tercon, terconazole (*n*=3 cells).

Figure 3. Molecular docking of drugs to the KCNT1 channel pore. A Structure of chicken KCNT1 in the active conformation (PDB:5U70)[24] with drugs docked to the channel pore domain, indicated by the yellow dashed box. **B** Molecular structures of active drugs identified in this study. **C** Individual active drugs docked to the KCNT1 pore domain as indicated. For clarity, only the S5, pore helix, selectivity filter, and S6 of each subunit is shown and rotated to best illustrate each drug binding mode. Threonine sidechains at the intracellular end of the selectivity filter are colored magenta, also the aspartate side chain in the S6 segment that interacts with atorvastatin.

Figure 4. Functional assessment of drug efficacy using inside-out patch clamping of HEK293T cells expressing WT KCNT1 channels. Single channel current traces were recorded at 0 mV and physiological K^+ gradient under control conditions and in the presence of different drugs: **A** Antrafenine (50 nM), **B** Nelfinavir mesylate (50 nM), **C** Atorvastatin (10 μM), and **D**. Regorafenib (10 μM). Insets show all-point amplitude histograms of the corresponding traces (C closed and O open levels).

Figure 5. Assessment of known drug efficacy in inhibiting KCNT1 channels carrying epilepsy-causing mutations, G288S, R398Q, and R928C. Concentration-response curves were constructed using KCNT1 currents (see Supplementary Fig. 3) recorded in inside-out patches in the presence of different concentrations of a drug in the bath and normalized to the current amplitude recorded before drug application. The data points were fitted with a Hill equation with a slope of -1. **A** Antrafenine, **B** Nelfinavir, and **C** Atorvastatin. (For IC_{50} values see Table 1)

Figure 6. Reduction of seizure phenotype in three *Drosophila* KCNT1 mutant lines by known drugs. The percentage of adult *Drosophila* showing seizure activity is shown for each of the KCNT1 mutant lines G288S, R398Q or R928C when raised on Normal Food (NF) or food with added Vehicle Control (VC), or the known drugs nelfinavir

mesylate, antrafenine, atorvastatin or regorafenib. Seizures in *Drosophila* are caused by expression of human *KCNT1* transgenes with mutations in the pore-adjacent loop domain, G288S (**A**), RCK1 domain, R398Q (**B**) or the RCK2 domain, R928C (**C**) in inhibitory GABAergic neurons. Data are presented as mean ± SEM.

F

Figure 1

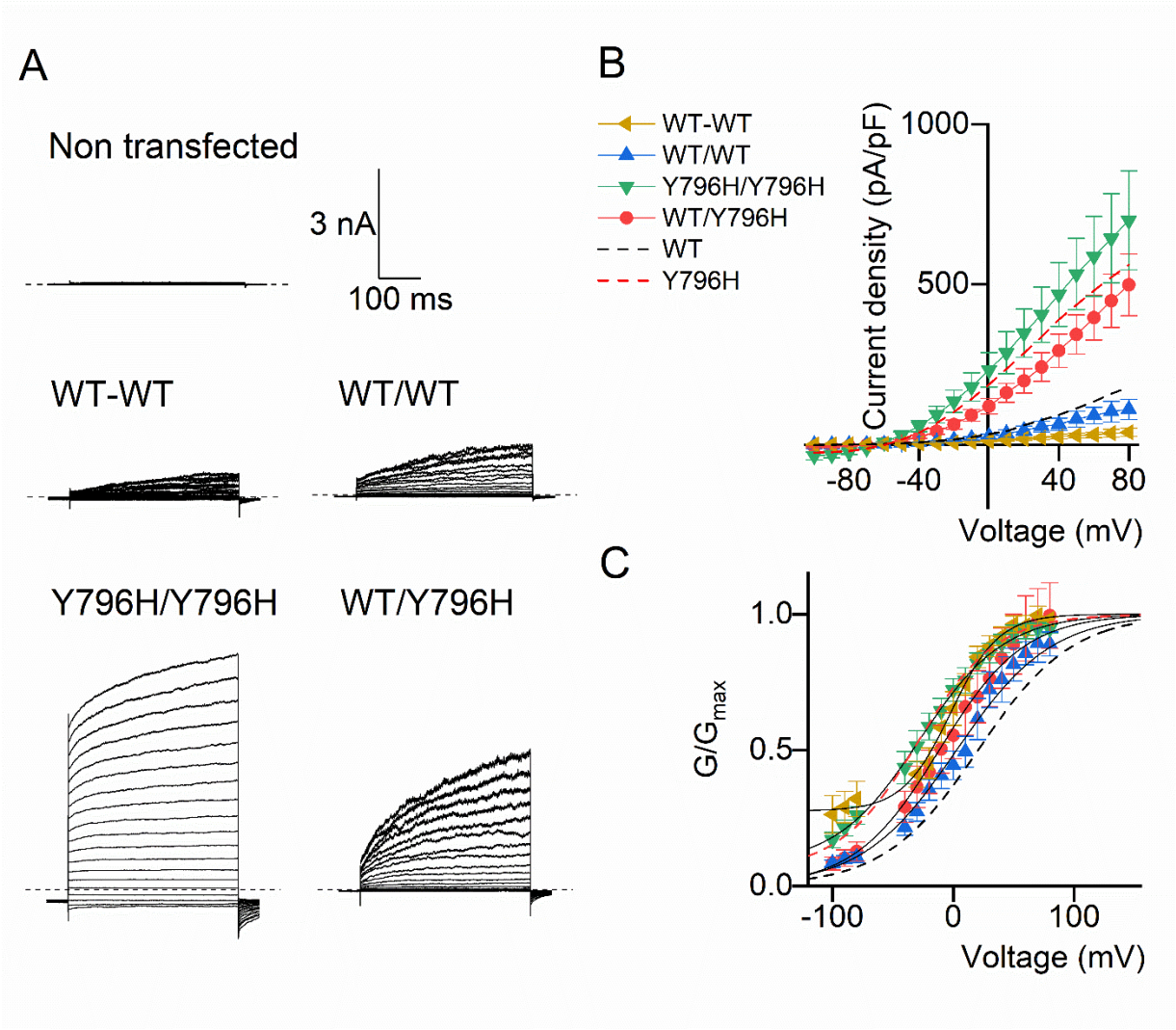
A
Non transfected
3 nA
100 ms
WT-WT
WT/WT
Y796H/Y796H
WT/Y796H
B
WT-WT
WT/WT
Y796H/Y796H
WT/Y796H
WT
Y796H
Current density (pA/pF)
1000
500
-80
-40
40
80
Voltage (mV)
C
G/G$_{max}$
1.0
0.5
0.0
-100
0
100
Voltage (mV)

Figure 2

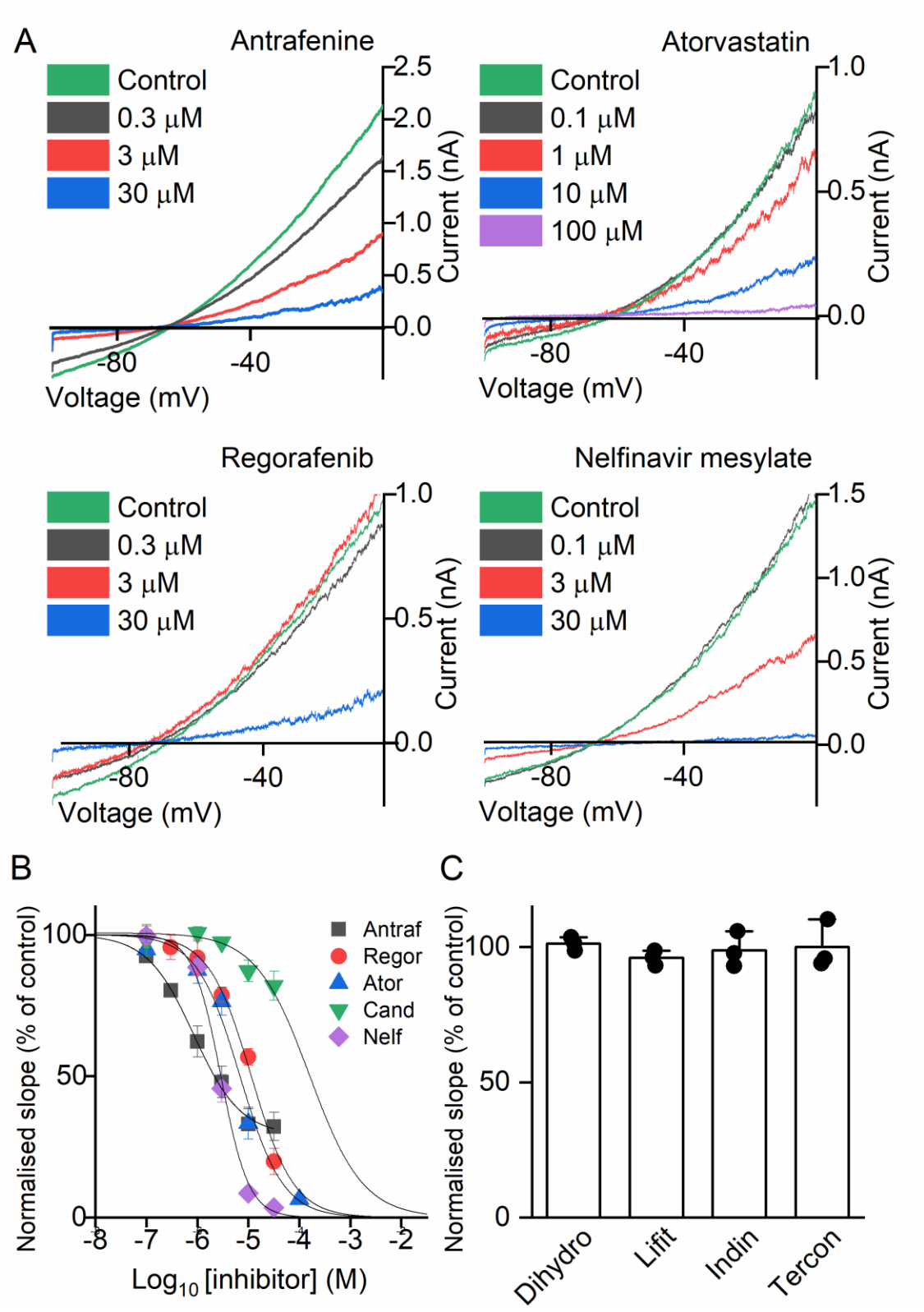
A
Antrafenine
Control
0.3 μM
3 μM
30 μM
Current (nA)
Voltage (mV)
Atorvastatin
Control
0.1 μM
1 μM
10 μM
100 μM
Current (nA)
Voltage (mV)
Regorafenib
Control
0.3 μM
3 μM
30 μM
Current (nA)
Voltage (mV)
Nelfinavir mesylate
Control
0.1 μM
3 μM
30 μM
Current (nA)
Voltage (mV)
B
Normalised slope (% of control)
Antraf
Regor
Ator
Cand
Nelf
Log10 [inhibitor] (M)
C
Normalised slope (% of control)
Dihydro
Lift
Indin
Tercon

Figure 3

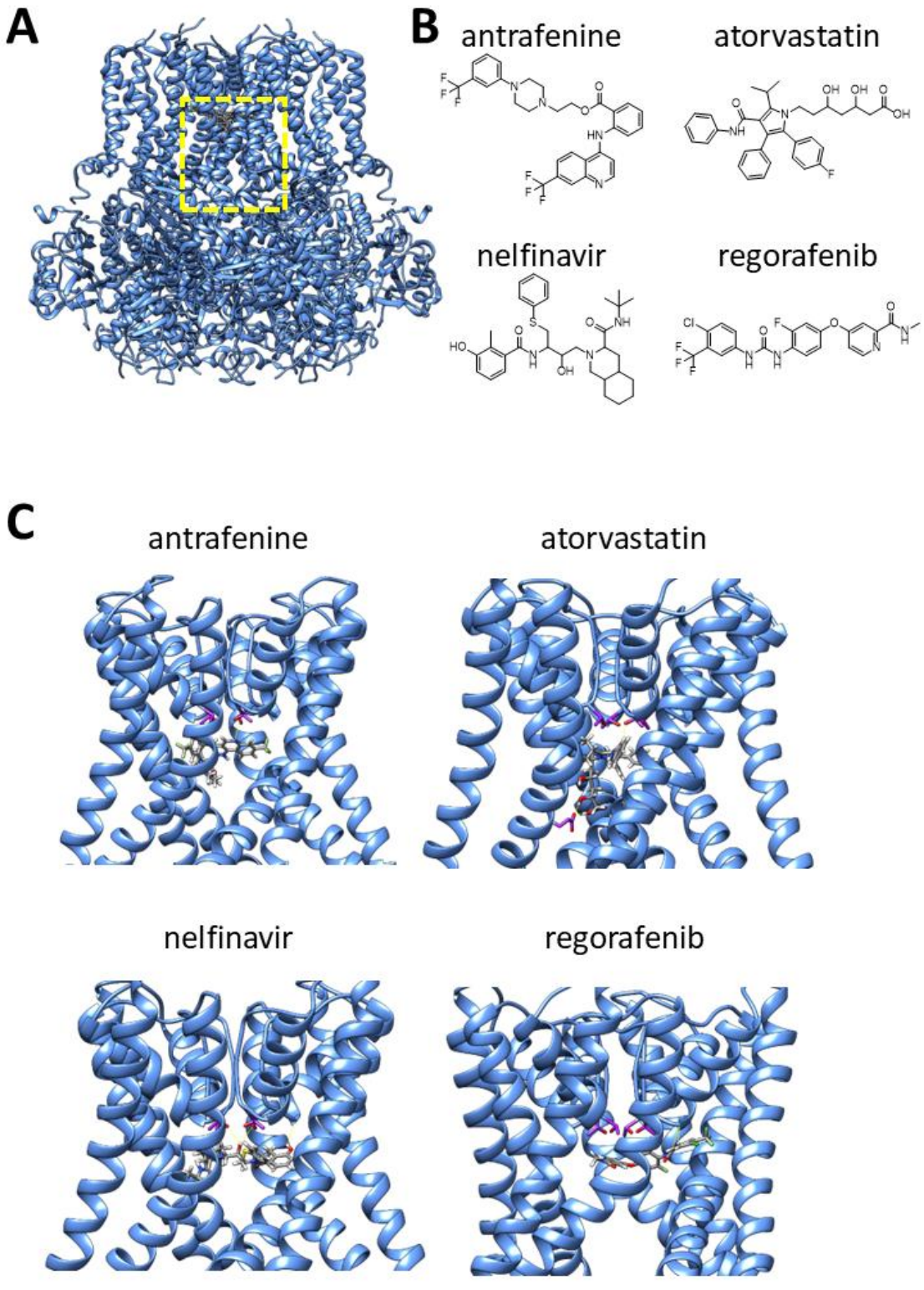
A
B
antrafenine
atorvastatin
nelfinavir
regorafenib
C
antrafenine
atorvastatin
nelfinavir
regorafenib

Figure 4

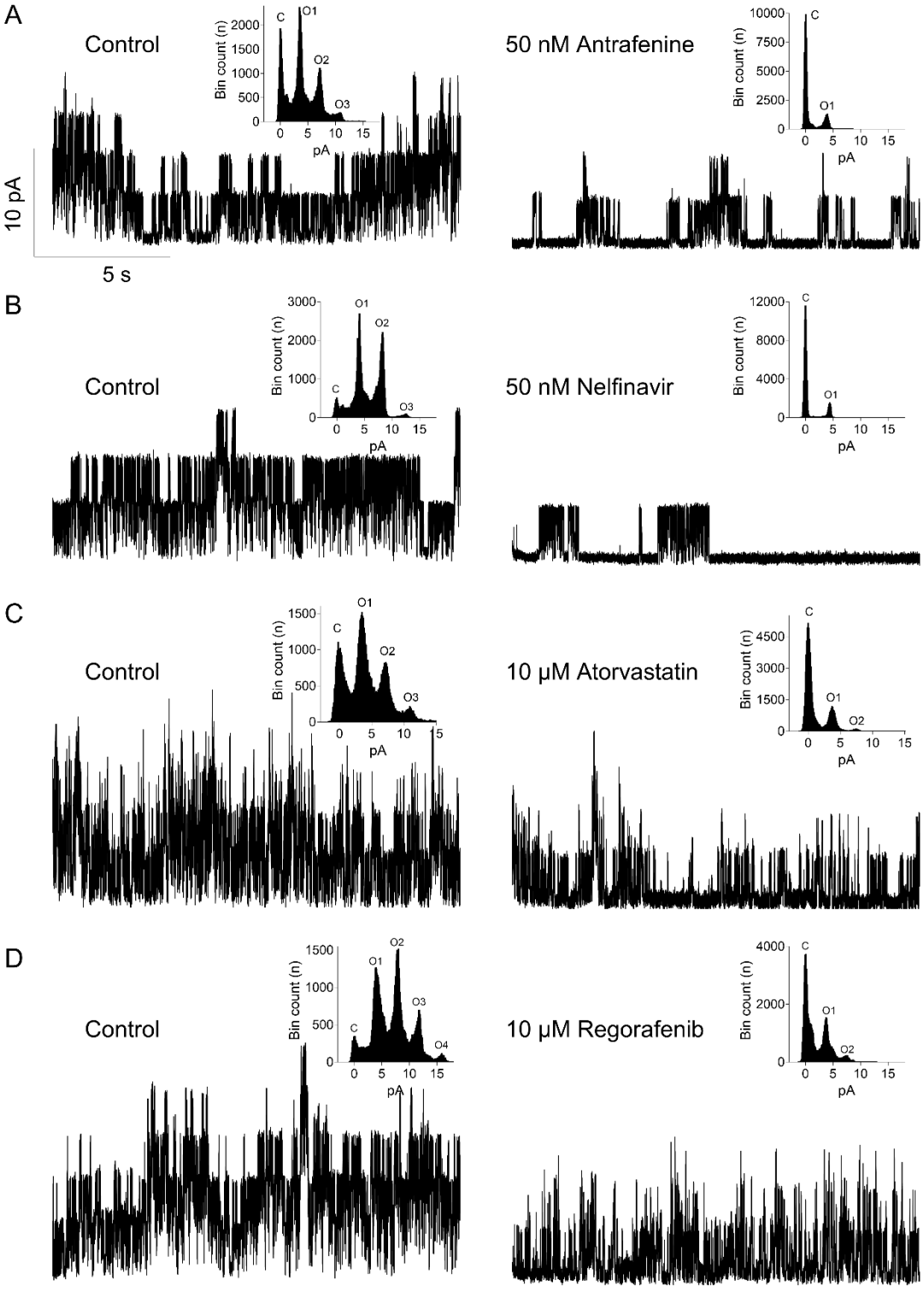
A
Control
50 nM Antrafenine
10 pA
5 s
B
Control
50 nM Nelfinavir
C
Control
10 µM Atorvastatin
D
Control
10 µM Regorafenib
Bin count (n)
pA
C
O1
O2
O3
O4

Figure 5

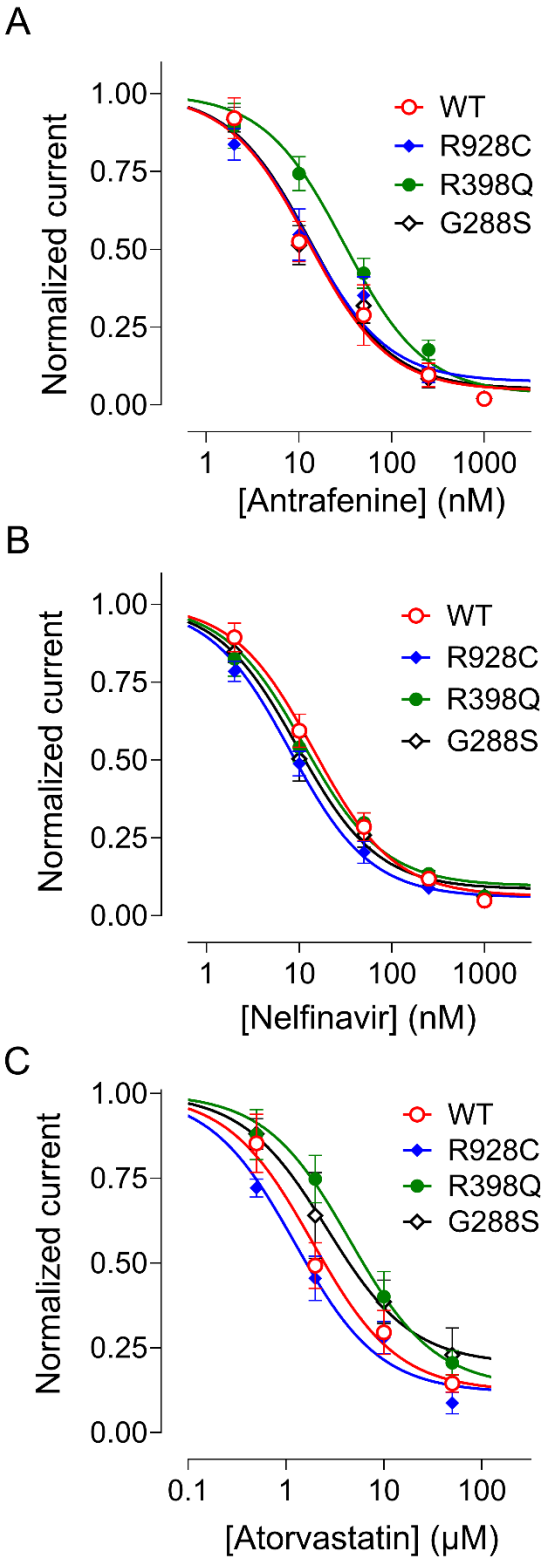
A
Normalized current
1.00
0.75
0.50
0.25
0.00
WT
R928C
R398Q
G288S
1
10
100
1000
[Antrafenine] (nM)
B
Normalized current
1.00
0.75
0.50
0.25
0.00
WT
R928C
R398Q
G288S
1
10
100
1000
[Nelfinavir] (nM)
C
Normalized current
1.00
0.75
0.50
0.25
0.00
WT
R928C
R398Q
G288S
0.1
1
10
100
[Atorvastatin] (μM)

Figure 6

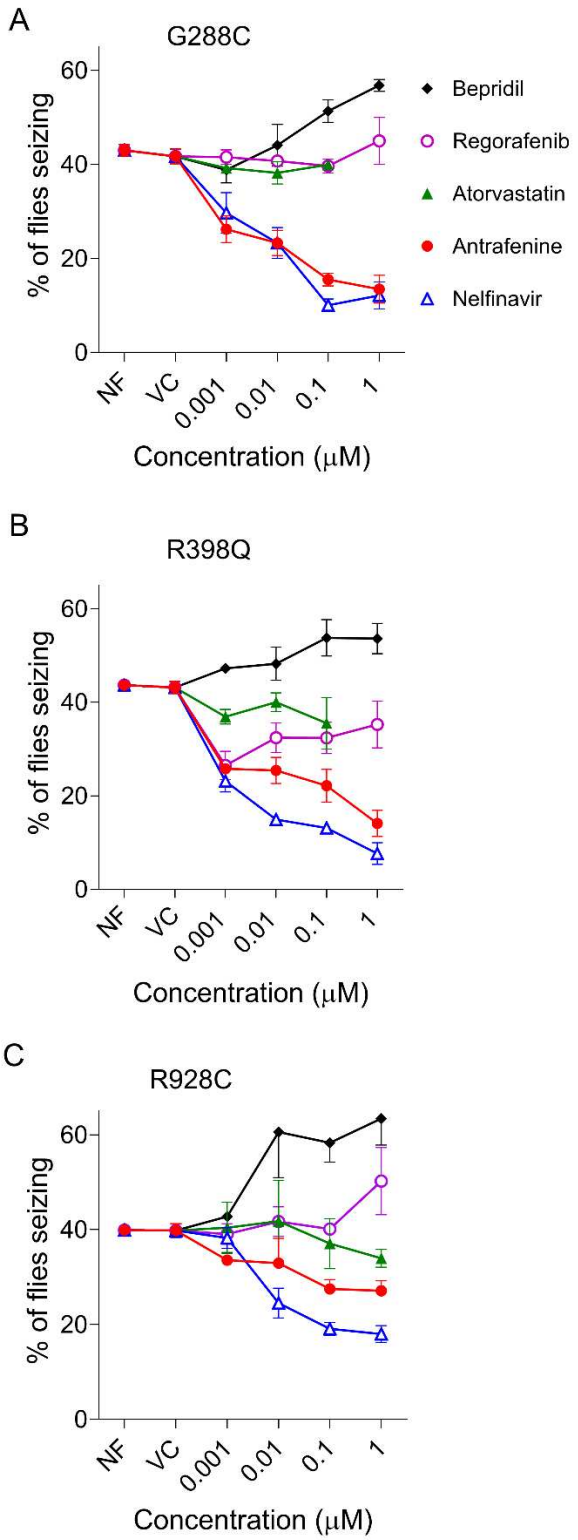
A
G288C
% of flies seizing
60
40
20
0
NF
VC
0.001
0.01
0.1
1
Concentration (μM)
Bepridil
Regorafenib
Atorvastatin
Antrafenine
Nelfinavir
B
R398Q
% of flies seizing
60
40
20
0
NF
VC
0.001
0.01
0.1
1
Concentration (μM)
C
R928C
% of flies seizing
60
40
20
0
NF
VC
0.001
0.01
0.1
1
Concentration (μM)

Identification of new KCNT1-epilepsy drugs by *in silico,* cell and *Drosophila* modelling

Supplementary Results and Methods

Supplementary Table 1: Parameters derived from Boltzmann analysis of WT, Y796H, and concatemeric $K_{Na}1.1$ currents.

Data are the mean ± SEM (of *n* number of cells provided in 5th column) half-maximal activation voltages ($V_{½}$) and apparent gating charge (*z*, obtained from the slope $k = RT/zF$) the Boltzmann function fitted to conductance-voltage plots. Currents were recorded from CHO cells transiently transfected with plasmids to form homotetrameric WT or Y796H $K_{Na}1.1$ channels, or with concatemeric homomeric or heteromeric constructs. A hypthen "-" between the subunits indicates the tethered tandem dimer (linker: GGGSGGGS) and the forward slash (/) between the subunits indicates that they are linked by the cleavable T2A motif (linker: GSGEGRGSLLTCGDVEENPG).

KCNT1 construct	Linker	$V_{½}$ (mV)	*z*	*n*
WT	none	7.38 ± 4.35	1.01 ±0.13	6
WT-WT	Tethered dimer	-15.72 ± 1.85	1.46 ±0.17	5
WT/WT	Cleavable T2A	-2.74 ± 7.69	0.89 ±0.07	5
Y796H	none	-39.99 ± 2.27	0.92 ±0.08	6
Y796H-Y796H	Tethered dimer	-50.83 ± 5.26	0.92 ±0.16	5
Y796H/Y796H	Cleavable T2A	-42.19 ± 7.97	0.82 ±0.12	5
WT/Y796H	Cleavable T2A	-16.42 ± 8.97	0.71 ±0.09	6
Y796H/WT	Cleavable T2A	-21.51 ± 5.86	0.80 ±0.08	6

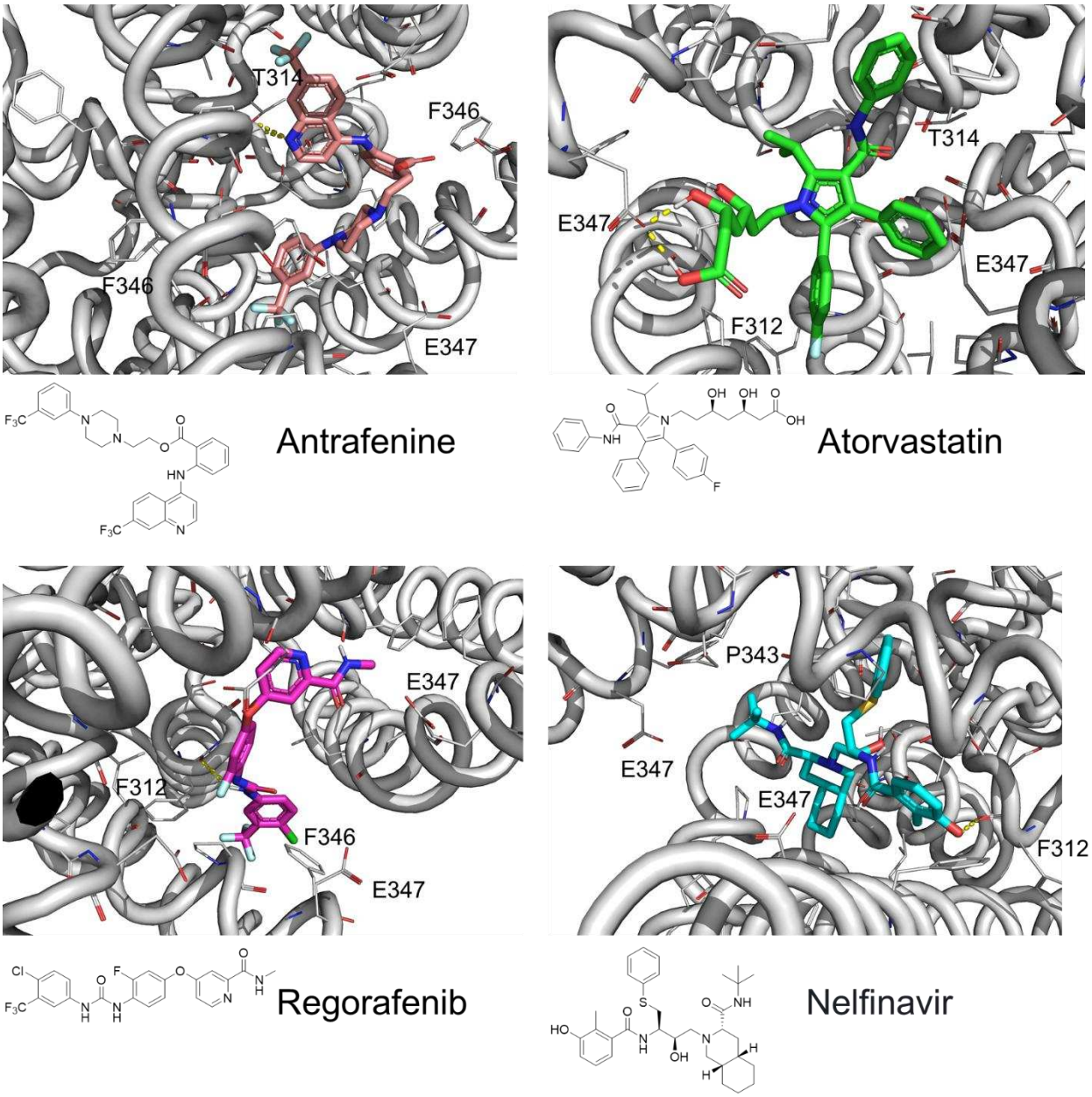

Supplementary Figure 1: Predicted interactions of drugs with the $K_{Na}1.1$ pore domain (PDB: 5U70) though molecular docking in Glide (Schrödinger).

Supplementary Table 2. Computationally-derived predicted properties of drugs using Schrödinger software. Glide docking scores for drugs interacting with the chicken activated KCNT1 channel structure (PDB: 5U70) and the inhibitor-bound human KCNT1 channel structure (PDB:8HKQ), and QikProp predictions of blood-brain-barrier (BBB) permeability (QPlogBB) and overall CNS activity (CNS). Docking scores that are more negative predict a higher affinity. QPlogBB values are the predicted logarithm of BBB partition coefficient, with positive values consistent with drugs that have good penetrance. CNS scores are between -2 (likely CNS inactive) to 2 (likely CNS active).

	Glide docking scores		**QikProp values**	
Drug	**Chicken**	**Human**	**QPlogBB**	**CNS**
Antrafenine	-8.88	-8.25	0.248	1
Atorvastatin	-7.59	-5.90	-2.092	-2
Nelfinavir	-8.01	-8.22	-0.849	-1
Regorafenib	-7.88	-8.32	-0.933	-1

A

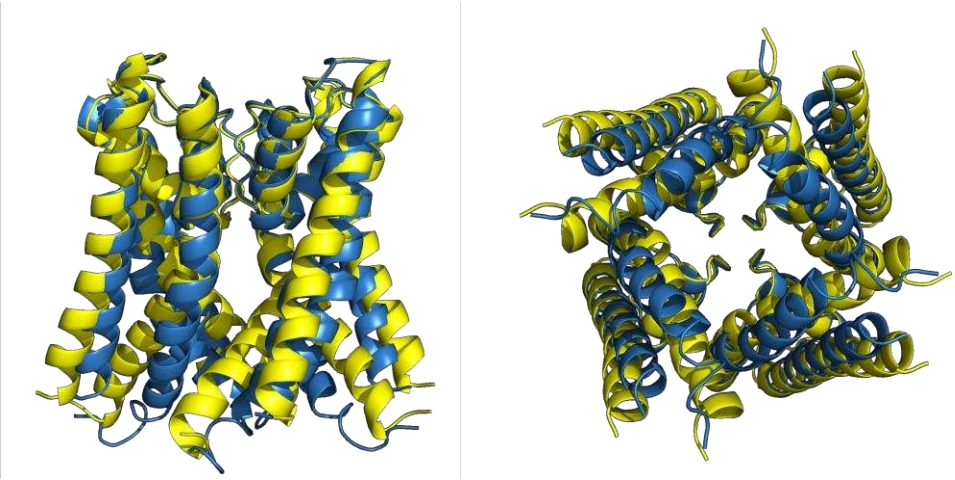

B

```
          <-------------S5------------>      <-----PH----->
Gga   244SAMFNQVLILICTLLCLVFTGTCGIQHLERAGEKLSLFKSFYFCIVTFS
Hsa   265SAMFNQVLILFCTLLCLVFTGTCGIQHLERAGENLSLLTSFYFCIVTFS

       <-SF->     <--------------S6------------->
Gga   TVGYGDVTPKIWPSQLLVVIMICVALVVLPLQFEELVYLWMERQKSGG340
Has   TVGYGDVTPKIWPSQLLVVIMICVALVVLPLQFEELVYLWMERQKSGG361
```

Supplementary Figure 2. Conservation in the pore domain between the chicken and human KCNT1 structures. A Three-dimensional alignment of pore domains from the structures of chicken (yellow, PDB:5U70) and human (blue, PDB:8HIR) active KCNT1. The root mean square deviation between atoms is 1.3 Å. **B** Sequence alignment of the chicken (*Gga*) and human (*Hsa*) KCNT1 pore domains indicated in **A** comprising the S5 and S6 transmembrane segments, the pore helix (PH), and selectivity filter (SF) as indicated. Differences between species are highlighted in yellow.

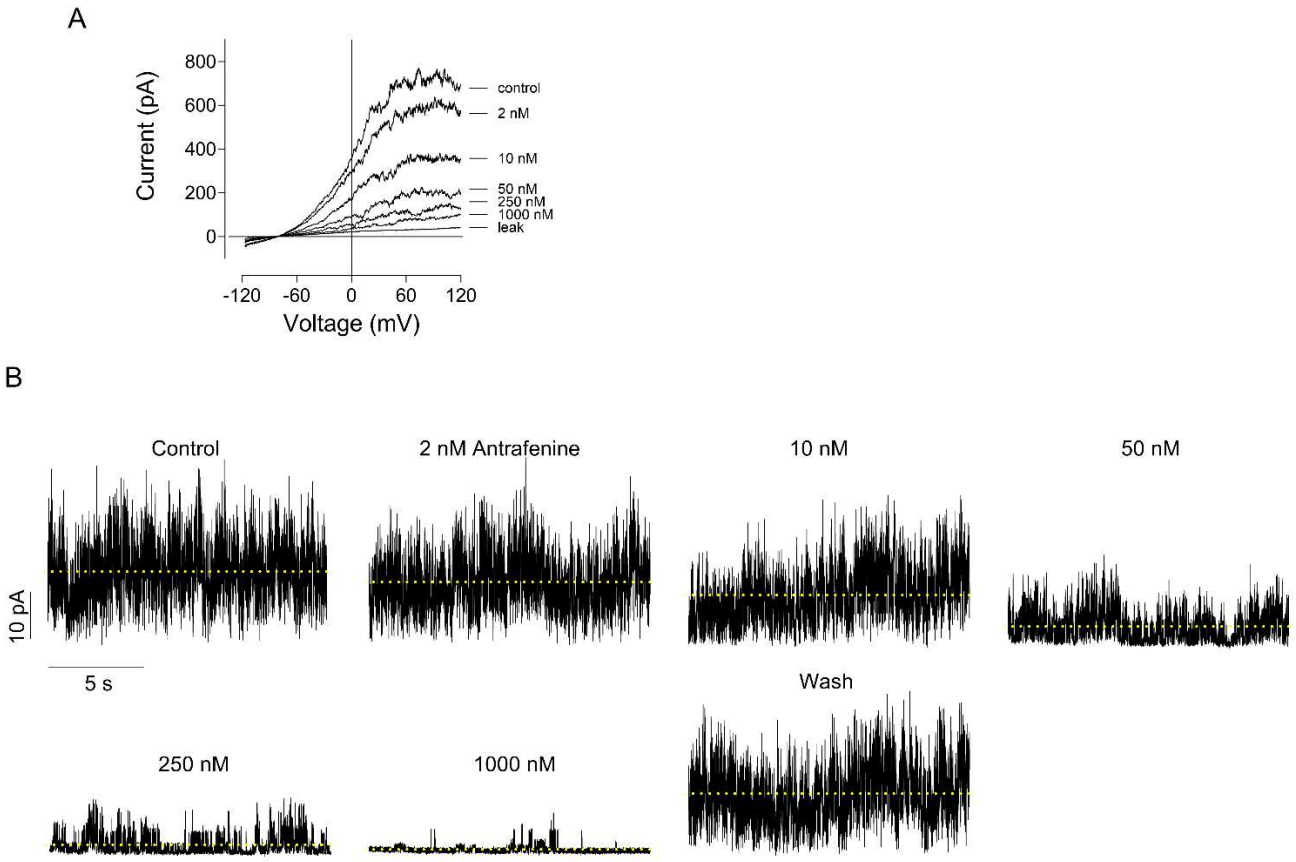

Supplementary Figure 3. Examples of the current traces used to build concentration-response curves. A Macroscopic G288S KCNT1 currents recorded in the inside-out patch in the presence of different concentrations of nelfinavir. Leak current was determined by replacing KCl in the bath solution with equimolar amount of NaCl. **B** Recording of a current in an inside-out patch containing 10 – 15 R398Q KCNT1 channels in the presence of different concentrations of Antrafenine, at 0 mV. The dashed lines represent the mean current amplitude of each trace.

Supplementary Table 3. One-way ANOVA results from the analysis of the Drosophila seizure phenotype data presented in Figure 6. ns - not significant.

G288S					
	Antrafenine	Nelfinavir	Atorvastatin	Regorafenib	Bepridil
F	44.78	52.39	1.529	0.7738	7.947
P value	<0.0001	<0.0001	0.2317	0.5799	0.0002
P summary	****	****	ns	ns	***
R squared	0.8924	0.8881	0.2342	0.1621	0.6234

R398Q					
	Antrafenine	Nelfinavir	Atorvastatin	Regorafenib	Bepridil
F	25.10	68.90	3.880	8.160	4.379
P value	<0.0001	<0.0001	0.0192	0.0002	0.0069
P summary	****	****	*	***	**
R squared	0.8451	0.9323	0.4630	0.6602	0.5104

R928C					
	Antrafenine	Nelfinavir	Atorvastatin	Regorafenib	Bepridil
F	5.341	35.92	0.8976	1.970	8.246
P value	0.0001	<0.0001	0.4932	0.1076	<0.0001
P summary	***	****	ns	ns	****
R squared	0.3022	0.7623	0.1108	0.2196	0.5076

Supplementary Table 4. P values obtained using One way ANOVA with Dunnett's multiple comparisons test of the data presented in Figure 6. Blue asterisks denote the statistically significant decrease in seizures compared to vehicle control, whereas red asterisks denote significant increase. ns – not significant. N is the number of independent experiments; number in brackets is the total number of flies analysed in each condition. For the controls, the number of independent experiments and the total number of flies for G288S, R398Q and R928C are 8 (88), 7 (141) and 12 (140), respectively.

	G288S					**R398Q**					**R928C**				
[µM]	**Antraf**	**Nelf**	**Atorv**	**Regor**	**Bepr**	**Antraf**	**Nelf**	**Atorv**	**Regor**	**Bepr**	**Antraf**	**Nelf**	**Atorv**	**Regor**	**Bepr**
0.001	<0.0001 **** N=4 (79)	0.0052 ** N=4 (54)	0.3267 ns N=4 (136)	>0.9999 ns N=2 (108)	0.5514 ns N=4 (85)	0.0003 *** N=3 (62)	<0.0001 **** N=5 (261)	0.0359 *** N=5 (113)	0.0002 *** N=4 (135)	0.5430 ns N=4 (95)	0.6765 ns N=4 (54)	0.9534 ns N=12 (170)	0.9998 ns N=4 (59)	0.9997 ns N=5 (56)	0.9923 ns N=4 (46)
0.01	<0.0001 **** N=5 (143)	<0.0001 **** N=5 (71)	0.1480 ns N=4 (114)	0.9929 ns N=4 (54)	0.9968 ns N=4 (78)	<0.0001 **** N=6 (126)	<0.0001 **** N=4 (119)	0.5236 ns N=4 (122)	0.0206 * N=4 (57)	0.3394 ns N=4 (74)	0.4387 ns N=6 (102)	<0.0001 **** N=6 (115)	0.9936 ns N=4 (67)	0.9865 ns N=5 (56)	0.0296 * N=3 (57)
0.1	<0.0001 **** N=5 (101)	<0.0001 **** N=10 (153)	0.7150 ns N=2 (103)	0.9009 ns N=3 (145)	0.0781 ns N=3 (78)	<0.0001 **** N=5 (144)	<0.0001 **** N=2 (77)	0.0676 ns N=2 (89)	0.0386 * N=3 (175)	0.0152 * N=3 (66)	0.0041 ** N=13 (216)	<0.0001 **** N=11 (177)	0.9720 ns N=4 (64)	>0.9999 ns N=4 (55)	0.0049 ** N=8 (110)
1	<0.0001 **** N=4 (56)	<0.0001 **** N=5 (73)		0.7301 ns N=3 (64)	0.0005 *** N=4 (65)	<0.0001 **** N=3 (71)	<0.0001 **** N=8 (113)		0.1793 ns N=3 (70)	0.0080 ** N=4 (55)	0.0006 *** N=24 (301)	<0.0001 **** N=11 (161)	0.3850 ns N=8 (118)	0.0360 * N=5 (63)	0.0002 *** N=9 (140)

PHARMACOKINETICS AND BRAIN UPTAKE OF ANTRAFENINE

Plasma pharmacokinetics and brain uptake of antrafenine was analyzed in male C57BL/6 mice by the Monash University Centre for Drug Candidate Optimisation. Antrafenine was administered intravenously at 1 mg/kg and 3 mg/kg into the tail vein and plasma was collected over a 24 h sampling period (n=3 mice/time point). Following administration, brain was harvested at four times over 24 hours and snap frozen in dry ice and subsequently stored frozen (-80°C) until analysis. The concentration of antrafenine was determined using liquid chromatography–mass spectrometry (LC-MS).

Summary of findings

The half-life of a 3 mg/kg IV administration of antrafenine in plasma was 7.4 hours. Given this, 4 hrs post IV administration of 3 mg/kg Antrafenine was taken as a representative time to compare plasma and brain concentrations. At 4 hrs we determined a mean plasma concentration of 47.5 nM ($\pm$5.9 nM SD) and a mean brain concentration of 13.9 nM ($\pm$3 nM SD). This showed significant penetration of Antrafenine into the brain at concentrations close to 30% of those present in plasma. This is clinically significant as the direct IC_{50} for antrafenine on single KCNT1 channels in inside-out patches was in the 10 nM range with an almost 90% inhibition at 300 nM. Historically, studies have shown that administering 900 mg/day which is approximately 12 mg/kg for a 75 kg adult resulted in a mean plasma concertation of 202 nM (Berry *et al*, 1983). As such, administration of Antrafenine should reach therapeutic concentrations higher than this IC_{50}.

Methods

Plasma pharmacokinetics and brain uptake of antrafenine

The systemic exposure of antrafenine was studied in non-fasted male C57BL/6 mice weighing 19.8 – 24.6 g. Mice had access to food and water *ad libitum* throughout the pre- and post-dose period. Antrafenine hydrochloride Mw 588.554 (Lot#10-KSS-51-2) was obtained from Toronto Research Chemicals/LGC Standards, Canada, and was dissolved in vehicle; 5% (v/v) DMSO, 25% (v/v) 40% (w/v) Trappsol in 0.9% (w/v) saline, 70% (v/v) 40 mM citrate buffered saline at pH 3.5 at concentrations of 0.5 mg/mL and 1.5 mg/mL.

On the day of dosing, each formulation was prepared by dissolving solid antrafenine in DMSO using vortexing and sonication prior to addition of 40% (w/v) Trappsol in 0.9% (w/v) saline followed by 40 mM citrate-buffered saline at pH 3.5. Each sample was vortexed to create a colorless / light yellow solution and was filtered through a 0.22 µm syringe filter prior to dosing.

Administration of antrafenine was performed by a single bolus IV injection into the tail vein of C57BL/6 male mice using a 1ml syringe with a 25G x 1” needle at a volume of 2 mL/kg. Each

formulation was dosed to mice by bolus injection into the lateral tail vein (2 mL/kg) and blood samples were collected at 1, 2, 5, 15 and 30 min; 1, 2, 4, 7.5 and 24 h post-dose (n=3 mice per time point for each formulation). A maximum of three blood samples were obtained from each mouse, with plasma samples being taken via submandibular bleed (approximately 120 µL). Blood was collected into polypropylene Eppendorf tubes containing heparin as anticoagulant and stabilization cocktail (Complete® (containing a protease inhibitor cocktail and EDTA) and potassium fluoride) to minimize the potential for *ex vivo* compound degradation in blood/plasma samples. Once collected, blood samples were centrifuged immediately, supernatant plasma was removed, snap frozen in dry ice and stored at -80°C until analysis by LC-MS. In addition, at the 15 min, 1, 4 and 24 h post-dose time points, the whole brain was rapidly removed from the carcass soon after the blood collection. The whole brains were blotted to remove excess blood, placed into pre-weighed polypropylene vials and weighed. The brains were snap frozen in dry ice and subsequently stored frozen (-80°C) until analysis.

Bioanalytical method for quantification of Antrafenine by LC-MS

The concentrations of antrafenine in each formulation were determined via a suitably validated generic HPLC-UV assay using a Waters Acquity HPLC system with a Phenomenex Ascentis Express RP-Amide column (50 x 2.1 mm, 2.7 µm) coupled to a Waters PDA detector analyzing at 254 nm. The measured concentrations in each formulation were within 15% of the nominal concentrations, hence the nominal doses were used for data analysis.

Test compound quantitation was performed by comparison of the response to that for a set of calibration standards prepared in the calibration matrix stated in Supplementary Table 5. A stock solution of test compound was spiked into an intermediate solvent containing 50% acetonitrile in water (v/v). Calibration standards were prepared by spiking the calibration matrix with the test compound solution standards and internal standard, maintaining the same final concentration of acetonitrile in all. The extraction from samples and standards was conducted in an equivalent manner using the extraction solvent and ratio described below.

Samples were analyzed on a Waters Xevo TQS Micro coupled to a Waters Acquity UPLC instrument in positive electrospray ionization multiple-reaction monitoring mode for detection, after passing through an ACQUITY UPLC BEH column (50 x 2.1 mm, 1.7 µm) at 40°C with LC conditions of; injection volume of 0.5 µL and a flow rate of 0.8 mL/min. The mobile phase consisted of (A) 0.05% formic acid in water and (B) 0.05% formic acid in acetonitrile delivered by gradient elution from 0 to 95% acetonitrile over 2 minutes. For plasma samples protein precipitation was performed using 80% acetonitrile in water at a 1:5 volume ratio. For brain samples protein precipitation was performed using acetonitrile at a 1:3 volume ratio.

Standards and samples were vortexed, centrifuged and the supernatant was collected for analysis. Analysis was conducted using the instrument conditions described above. Analytical replicates (ARs) were prepared similarly to the calibration standards at three concentrations, and repeat injections of these were included throughout the analytical run to assess assay performance. A summary of the assay validation details is included in Supplementary Table 5.

Supplementary Table 5: Validation of antrafenine detection range using liquid chromatography-mass spectrometry.

Analyte	Antrafenine			
Matrix	**Parameter**	**AR (ng/ml)**	**Accuracy (% bias)**	**Precision (%RSD)**
Mouse Plasma	**Accuracy and Precision [a]**	50 (n=6)	1.5	5.4
		500 (n=6)	0.2	6.1
		2000 (n=6)	-1.3	3.6
	Calibration ^	**Range (ng/ml)**	**R^2**	**LLQ 9ng/ml)[b]**
		1 - 10000	0.9969	1.0
	Recovery and matrix factor [c]	**Recovery (%)**	**Matrix factor (%)**	**Stability**
		108.7	-15.3	Not assessed
^ calibration data were fitted to a linear equation with a weighting factor of 1/x2				
Matrix	**Parameter**	**AR (ng/ml)**	**Accuracy (% bias)**	**Precision (%RSD)**
Brain Tissue Homogenate	**Accuracy and Precision [a]**	50 (n=6)	3.2	5.3
		500 (n=6)	0.3	2.2
		2000 (n=6)	-1.2	1.0
	Calibration ^	**Range (ng/ml)**	**R^2**	**LLQ 9ng/ml)[b]**
		1 - 5000	0.998	1
	Recovery and matrix factor [c]	**Recovery (%)**	**Matrix factor (%)**	**Stability [d]**
		102.2	6.6	107.4
^ calibration data were fitted to a linear equation with a weighting factor of 1/x.				

[a] Acceptance criteria for batch analysis: at least 67% of the AR samples must be within ±15% of nominal values (CDCO In-house acceptance criteria).

[b] The lower limit of quantitation (LLQ) was defined by the lowest acceptable calibration standard for which the back calculated concentration was within ±20% of the nominal concentration.

[c] For plasma, recovery and matrix factor values calculated as an average of four points (10, 50, 500 and 5000 ng/mL). For brain homogenate, recovery and matrix factor and stability values calculated as an average of three technical replicates, at a single point (500 ng/mL).

[d] Stability was assessed for the period of brain sample processing (15 min).

Standard Calculations

The measured concentrations in each of the formulations were within 15% of the nominal concentrations, hence the nominal doses were used for data analysis.

The plasma concentration versus time profile was defined by the average plasma concentration at each sample time, and PK parameters were calculated using non-compartmental methods

(PKSolver Version 2.0). Standard calculations for each pharmacokinetic parameter are listed below.

$$\text{Plasma CL} = \frac{\text{Dose}_{\text{IV}}}{\text{AUC}_{\text{IV},0-\text{inf}}} \qquad \text{Plasma V}_{ss} = \frac{\text{AUMC}_{\text{IV},0-\text{inf}}}{\text{AUC}_{\text{IV},0-\text{inf}}} \times \text{Plasma CL} \qquad t_{1/2} = \frac{Ln(2)}{\lambda_z}$$

CL Clearance in plasma/blood after IV administration

$AUC_{IV,0\text{-}inf}$, Area under the plasma concentration versus time profile from time zero to infinity after IV administration

$t_{1/2}$ Elimination half-life

λ_z Terminal elimination rate constant after IV administration

V_s Apparent volume of distribution in plasma/blood at steady state

$AUMC_{IV,0\text{-}inf}$, Area under the first moment of the plasma concentration versus time profile from time zero to infinity after IV administration

Calculation of Brain Exposure Parameters

The concentration of antrafenine in brain parenchyma was calculated based on the measured concentration in brain homogenate, after correcting for the contribution of compound contained within the vascular space of brain samples as follows:

$C_{brain} = C_{brain\ homogenate} - C_{brain\ vasculature}$ where $C_{brain\ vasculature} = C_{plasma} \times V_p$

C_{brain} = concentration of compound in brain parenchyma (ng/g)

$C_{brain\ homogenate}$ = concentration of compound in brain homogenate (ng/g)

$C_{brain\ vasculature}$ = concentration of compound in brain vasculature (ng/g)

C_{plasma} = concentration of compound in plasma (ng/ml)

V_p = brain plasma volume (17 µL/g for male C57BL/6 mice; Nicolazzo et al, (2010),

Clinical and Experimental Pharmacology and Physiology, **37**, 647-649).

For each mouse, the brain-to-plasma (B:P) concentration ratio (based on total concentrations in each matrix) was calculated as: Brain: plasma = C_{brain} / C_{plasma}. Concentrations in brain were measured as ng/g of tissue, and are presented herein with units of µM, which assumes a sample density of 1 g/mL.

Results

Plasma pharmacokinetics and brain uptake of antrafenine

No adverse reactions or compound-related side effects were observed in any mice following IV administration of antrafenine at 1 and 3 mg/kg. Plasma and brain concentration versus time profiles are presented in Supplementary Fig. 4, with pharmacokinetic parameters and brain

concentrations for individual mice, together with corresponding values for the brain-to-plasma (B:P) ratio are provided in Supplementary Tables 6 and 7, respectively.

Following IV administration at 1 and 3 mg/kg, concentrations of antrafenine in plasma remained measurable for the duration of the 24-hour sampling period, and each profile exhibited an apparent terminal half-life of approximately 7 h. Based on the plasma AUC values, the exposure increased in proportion to the 3-fold increase in dose from 1 to 3 mg/kg. The apparent plasma clearance was low and the volume of distribution was high.

Concentrations of antrafenine in brain were quantifiable at 15 min, 1 and 4 h post-dose, however compound was not detected in brain at 24 h at either dose level. The apparent increase in B:P ratio between 15 min and 4 h suggests that distributional equilibrium between brain and plasma was not achieved instantaneously, and the value at 4 h is likely to provide a better approximation of the steady-state B:P ratio than the values at the earlier two timepoints.

Brain to plasma ratios across the post-dose period were quite consistent at the two dose levels of 1 and 3 mg/kg.

Supplementary Table 6: Pharmacokinetic parameters for antrafenine in male C57BL/6 mice following IV administration.

Parameter	IV administration at 1mg/kg	IV administration at 3mg/kg
Apparent $t_{1/2}$	7.3	7.4
Plasma $AUC_{0\text{-}inf}$ (h*μM)	1.29	3.14
Plasma CL (ml/min/kg)	22.0	27.1
Plasma VSS (L/kg)	2.30	3.90

Supplementary Table 7: Individual and mean ± SD (n = 3) plasma and brain concentrations, and brain-to-plasma (B:P) ratios, of antrafenine in male C57BL/6 mice following IV administration at 1 and 3 mg/kg.

Antrafenine (1 mg/kg)							
Time (h)	Mouse ID	Plasma Concentration (µM)		Brain Parenchyma Concentration (µM)		B:P ratio	
		Individual	Mean ± SD	Individual	Mean ± SD	Individual	Mean ± SD
0.25	1	0.313	0.297 ± 0.0569	0.0085	0.0133 ± 0.0075	0.027	0.050 ± 0.039
	2	0.233		0.0220		0.094	
	3	0.344		0.0095		0.028	
1	4	0.122	0.113 ± 0.0089	0.0105	0.0085 ± 0.0029	0.087	0.076 ± 0.027
	5	0.112		0.0052		0.046	
	6	0.104		0.0099		0.096	
4	7	0.0125	0.0131 ± 0.0008	0.0057	0.0039 ± 0.0018	0.46	0.30 ± 0.15
	8	0.014		0.0037		0.26	
	9	0.0129		0.0022		0.17	
24	10	0.0020	0.0018 ± 0.0002	ND	---	---	---
	11	0.0016		ND		---	
	12	0.0018		ND		---	
Antrafenine (3 mg/kg)							
Time (h)	Mouse ID	Plasma Concentration (µM)		Brain Parenchyma Concentration (µM)		B:P ratio	
		Individual	Mean ± SD	Individual	Mean ± SD	Individual	Mean ± SD
0.25	13	0.738	0.697 ± 0.0454	0.0311	0.0295 ± 0.0025	0.042	0.042 ± 0.0050
	14	0.705		0.0266		0.038	
	15	0.648		0.0309		0.048	
1	16	0.282	0.280 ± 0.0708	0.0402	0.0314 ± 0.0117	0.14	0.11 ± 0.028
	17	0.208		0.0182		0.087	
	18	0.349		0.0358		0.10	
4	19	0.053	0.0475 ± 0.0059	0.0173	0.0139 ± 0.0030	0.32	0.29 ± 0.039
	20	0.0419		0.0127		0.30	
	21	0.0471		0.0117		0.25	
24	22	0.0057	0.0065 ± 0.0020	ND	---	---	---
	23	0.0088		ND		---	
	24	0.0051		ND		---	

Supplementary Figure 4: Plasma and brain concentrations of antrafenine in male C57BL/6 mice following IV administration at 1 mg/kg (A) and 3 mg/kg (B). The dashed horizontal line represents the minimum detectable concentration of antrafenine.